

# Electronic properties of twisted multilayer graphene

V. Hung Nguyen<sup>1</sup>, Trinh X. Hoang<sup>2</sup> and J.-C. Charlier<sup>1</sup>

<sup>1</sup>*Institute of Condensed Matter and Nanosciences,  
Université catholique de Louvain (UCLouvain), B-1348 Louvain-la-Neuve, Belgium*

<sup>2</sup>*Institute of Physics, Vietnam Academy of Science  
and Technology, Ba Dinh, Hanoi 11108, Vietnam*

## Abstract

Twisted bilayer graphene displays many fascinating properties that can be tuned by varying the relative angle (also called twist angle) between its monolayers. As a remarkable feature, both the electronic flat bands and the corresponding strong electron localization have been obtained at a specific “magic” angle ( $\sim 1.1^\circ$ ), leading to the observation of several strongly correlated electronic phenomena. Such a discovery has hence inspired the creation of a novel research field called *twistronics*, i.e., aiming to explore novel physical properties in vertically stacked 2D structures when tuning the twist angle between the related layers. In this paper, a comprehensive and systematic study related to the electronic properties of twisted multilayer graphene (TMG) is presented based on atomistic calculations. The dependence of both the global and the local electronic quantities on the twist angle and on the stacking configuration are analyzed, fully taking into account atomic reconstruction effects. Consequently, the correlation between structural and electronic properties are clarified, thereby highlighting the shared characteristics and differences between various TMG systems as well as providing a comprehensive and essential overview. On the basis of these investigations, possibilities to tune the electronic properties are discussed, allowing for further developments in the field of *twistronics*.

PACS numbers:

## I. INTRODUCTION

Twisted multilayer graphene (TMG) refers to structures of vertically stacked graphene layers when one or a few layers are rotated relative to the others by arbitrary angles [1–11], thus creating the so-called moiré superlattices. The first member of TMG systems, twisted bilayer graphene (TBLG), has recently attracted great interest from the scientific community since it exhibits fascinating properties, leading to the exploration of several novel features as surprising as superconductivity that can not be observed in conventional graphene systems [12]. In particular and most remarkably, electronic properties of TBLG can be tuned by varying the twist angle  $\theta$  [13, 14], especially leading to the observation of localized flat bands near the Fermi level at a critical angle ( $\simeq 1.1^\circ$ ) called *the magic angle* [15, 16]. At this critical angle, many-body effects are therefore significantly enlarged [17–22] and charge carriers do not possess enough kinetic energy to escape from their strong mutual interactions, thus forming novel strongly correlated electronic states. Such a strong electronic correlation in magic-angle TBLG is the key ingredient for observing several novel phenomena such as superconductivity, correlated insulating states, magnetism, and even quantized anomalous Hall effects [23–32].

The observations mentioned above have been considered as real scientific breakthroughs, creating a nascent field of *twistronics* [33]. Indeed, after the discovery of magic-angle TBLG, the research of other twisted systems has become an emerging topic. In addition to TMG, the explored systems include also twisted superlattices of other 2D layered materials such as graphene on hexagonal boron nitride, graphene on transition-metal dichalcogenide layers, van der Waals moiré superlattices of transition-metal dichalcogenide layers, and so on (e.g., see Refs. [34–41] as well as the recent review [42] and references therein). These explorations have also inspired researchers to extendedly apply the twist approach to other physical systems, e.g., magnetic 2D materials [43–46] and photonic layered structures [47–50]. In overall, the properties of those systems are definitely dependent of their constituting layers and importantly, can be tuned by varying their twist angle, similar to those observed in TBLG. In particular, in the TMG cases, electronic flat bands and accordingly, the strongly correlated electronic phenomena have been similarly observed around their magic angle (e.g., see in Refs. [4, 8, 11, 51–53]). Moreover, more tunable possibilities can be observed in TMG [4–6, 8, 9, 25, 54, 55], due to a larger number of layers and the plenty of stacking

configurations [56], compared to TBLG. In this context, a comprehensive understanding of the electronic properties of TMG is highly desirable. Some new TMGs [6, 9, 11] have been very recently produced experimentally, and hence their corresponding electronic properties are needed to be more exhaustively clarified. In addition, a good understanding of those twisted systems could be also helpful for research of twisted structures based on other 2D materials.

On the theoretical side, though a large number of works devoted to the electronic properties of some TMG has been reported (e.g., in [14, 33, 51, 52, 57–59]), a systematical study on this subject is however still missing. Remarkably, it has been shown that atomic reconstruction (i.e., the structure relaxation) significantly occurs in TBLG at low angles ( $\lesssim 1.1^\circ$ ), thus strongly influencing their electronic properties, i.e., especially the formation of electronic flat bands as well as the electronic localization pictures [20, 60, 61]. The structural and electronic properties of TBLG also exhibit a strong correlation [61], that explains essentially the corresponding electronic localization features. Fully taking into account the atomic reconstruction effects is therefore mandatory to compute accurately the electronic properties of TMG, which has not been properly considered yet in all works previously published in the literature.

This paper aims to investigate systematically the most common and essential electronic properties of TMG by atomistic calculations, which fully take the atomic reconstruction into account. First, twisted bilayer graphene is investigated to illustrate the overall structural and electronic properties induced by the twisting effects. Some of these properties are commonly observed in other multilayer structures. Afterward, the study focuses on several typical twisted multilayer (more than 2 graphene layers) systems around their magic angles, at which electronic flat bands and strong electron localization are also observed. The correlation between the obtained electronic and structural properties is also clarified. Electronic (both global and local) quantities obtained depending on the twist angle and the stacking configuration are analyzed in details, thus highlighting the shared characteristics and differences between TMGs. Finally, on the basis of these investigations, possibilities to tune these electronic properties are discussed.

## II. MODELING METHODOLOGY

As mentioned earlier, the atomic reconstruction is significant and hence taking into account these structural effects is mandatory to model accurately the electronic properties of twisted graphene systems, especially, at small twist angles around and below the magic one. In this work, we used classical force-fields to compute the atomic structure relaxation. More specifically, intralayer forces are computed using the optimized Tersoff and Brenner potentials [62], while interlayer forces are modeled using the Kolmogorov-Crespi potentials [63, 64]. The atomic structure was optimized until all force components are smaller than 0.5 meV/atom and the electronic calculations were then performed. The atomic structure relax-

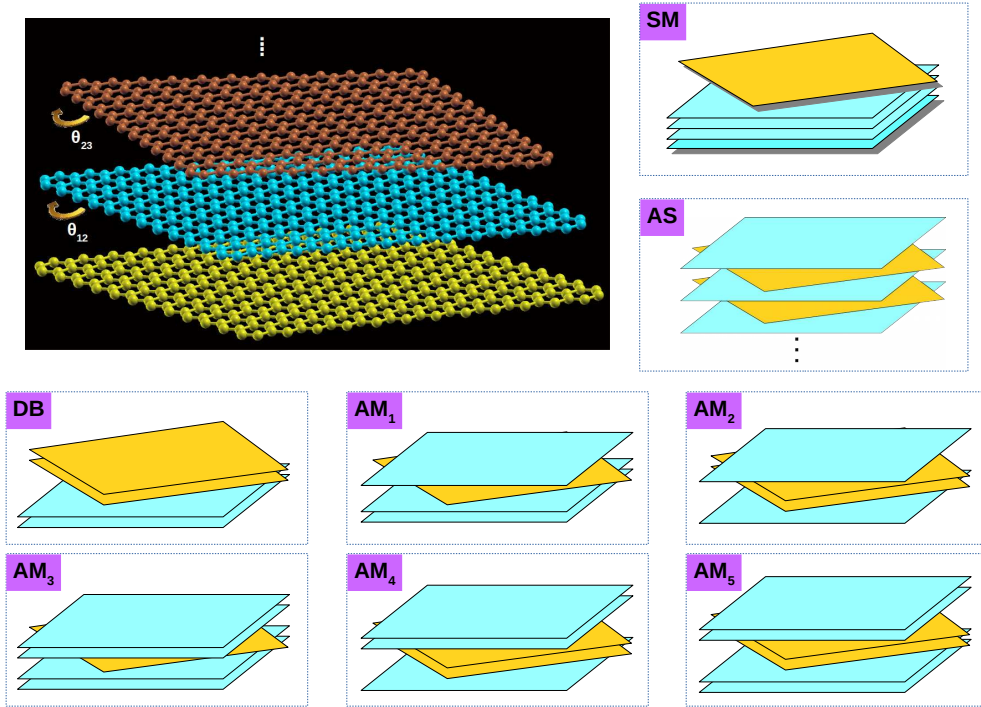


FIG. 1: Twisted multilayer graphene systems investigated in this work. SM-structures are twisted systems created by putting and rotating a graphene monolayer on top of a multilayer ( $n$  layers) graphene that is either in AB stacked or in ABC stacked. These structures are hereafter abbreviated as SM-(AB) <sub>$n$</sub>  and SM-(ABC) <sub>$n$</sub> , respectively. AS-structures are alternatively twisted systems of  $n$  graphene monolayers, abbreviated as AS <sub>$n$</sub> . DB is the abbreviation of twisted double bilayer graphene superlattices. At last, AM <sub>$n$</sub>  structures ( $n = 1,2,3,4,5$ ) are alternatively twisted systems containing, at least, one Bernal stacking graphene bilayer.

ation obtained by this method is shown to be in good agreement with experiments [18, 65–67] as well as the results obtained by other (both quantum and semi-classical) methods [60, 68–70], except that the intralayer equilibrium  $C$ - $C$  bond distance is slightly overestimated by  $\sim 1\%$  [64].

Similarly to previous works [20, 61], the electronic properties of TMG (schematized in Fig.1) were then computed using the  $p_z$  tight-binding (TB) Hamiltonians after the structural optimization has been fully achieved. Hopping energies  $t_{nm}$  between carbon  $C$ -sites are determined by the standard Slater-Koster formula

$$t_{nm} = \cos^2 \phi_{nm} V_{pp\sigma}(r_{nm}) + \sin^2 \phi_{nm} V_{pp\pi}(r_{nm}) \quad (1)$$

where the direction cosine of  $\vec{r}_{nm} = \vec{r}_m - \vec{r}_n$  along Oz axis is  $\cos \phi_{nm} = z_{nm}/r_{nm}$ . The distance-dependent Slater-Koster parameters are determined as [71]

$$\begin{aligned} V_{pp\pi}(r_{nm}) &= V_{pp\pi}^0 \exp \left[ q_\pi \left( 1 - \frac{r_{nm}}{a_0} \right) \right] F_c(r_{nm}) \\ V_{pp\sigma}(r_{nm}) &= V_{pp\sigma}^0 \exp \left[ q_\sigma \left( 1 - \frac{r_{nm}}{d_0} \right) \right] F_c(r_{nm}) \end{aligned}$$

with a smooth cutoff function  $F_c(r_{nm}) = \left[ 1 + \exp \left( \frac{r_{nm} - r_c}{\lambda_c} \right) \right]^{-1}$ .

In this work, the TB Hamiltonian was further simplified from the model considered in [61], i.e., only couplings limited by  $r_{inplane} \leq 2.16 \text{ \AA}$  were taken into account. This approximation presents an advantage that the matrix of TB Hamiltonian is very sparse so as to make calculations feasible for small twist angles and/or multilayer systems in which the number of  $C$  atoms could be huge. Within this approximation, the TB parameters [61] are slightly adjusted as follows:

$$\begin{aligned} V_{pp\pi}^0 &= -2.7 \text{ eV}, \quad V_{pp\sigma}^0 = 367.5 \text{ meV}, \\ \frac{q_\pi}{a_0} &= \frac{q_\sigma}{d_0} = 22.18 \text{ nm}^{-1}, \\ a_0 &= 0.1439 \text{ nm}, \quad d_0 = 0.33 \text{ nm}, \quad r_c = 0.614 \text{ nm}, \quad \lambda_c = 0.0265 \text{ nm} \end{aligned}$$

Indeed, such an adjusted TB Hamiltonian fairly accurately reproduces the electronic properties of TBLG as obtained in [61] as well as in experiments, e.g., in [20, 22, 23]. As a clear illustration, the almost flat bands near the Fermi level is perfectly reproduced in the relaxed TBLG in the vicinity of the magic angle (i.e.,  $\sim 1.1^\circ$ , see Fig. 3 below) as experimentally observed (e.g., see in Ref. [23]).

### III. TWISTED BILAYER GRAPHENE

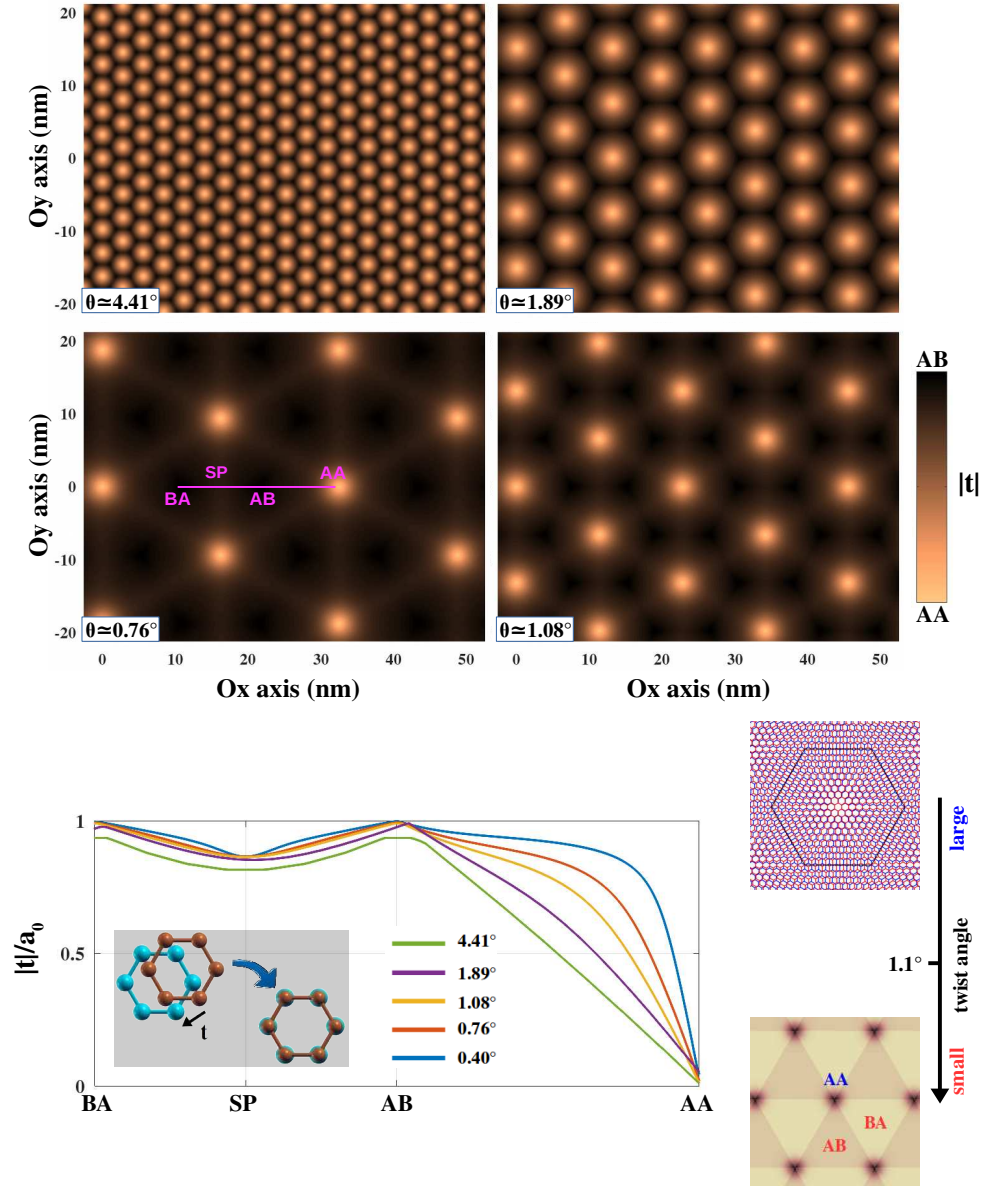


FIG. 2: Stacking structure of TBLG imaged by the spatial variation of stacking vector  $\mathbf{t}$  (as defined in the inset of bottom-left panel) when varying the twist angle  $\theta$ . Four top images are 2D real-space representation of  $|\mathbf{t}|$  while the bottom-left one is a plot of  $|\mathbf{t}|$  extracted along the line connecting BA - SP (soliton line) - AB - AA stacking regions. The bottom-right diagram is a simple description of the stacking properties of TBLG in the different  $\theta$ -regimes (from large to small twist-angles).

As the simplest TMG structure, TBLG exhibits most clearly essential electronic prop-

erties induced by the twisting effects. These properties as well as their correlation with the structural properties, that generally also appear in other TMGs (as examples, see in Refs. [52, 61] as well as illustration in Figs.14-15 in section V), will be therefore revised and systematized in this section.

Typical images illustrating the evolution of the stacking structure in TBLG when varying the twist angle  $\theta$  are presented in Fig.2. The stacking vector  $\mathbf{t}$ , as illustrated in the bottom-left panel, indicates the smallest displacement applied locally to one layer to recover the AA stacking at the considered position. In general, TBLG superlattice includes three typical stacking regions: AA stacking, AB/BA stacking regions and soliton lines between AB/BA ones (called SP for *saddle point*). The presented images illustrate that the magic angle  $\sim 1.1^\circ$  separates TBLG into two regimes:  $\theta > 1.1^\circ$  (large angles) and  $\theta < 1.1^\circ$  (small ones) [61]. At large angles, the moiré superlattice evolves smoothly and both AA and AB/BA stacking regions are continuously enlarged when decreasing the twist angle. However, AA stacking regions get saturation when  $\theta$  decreasingly approaches  $1.1^\circ$ . At small angles, whereas the size of AA stacking regions is unchanged, AB/BA regions are continuously enlarged when decreasing  $\theta$ , according to the enlargement of moiré cells. Thus, in addition to the critical angle (i.e., magic angle)  $\sim 1.1^\circ$ , there are two TBLG classes, separated by such angle and exhibiting distinct stacking structures, as summarized in the bottom-right diagram of Fig.2.

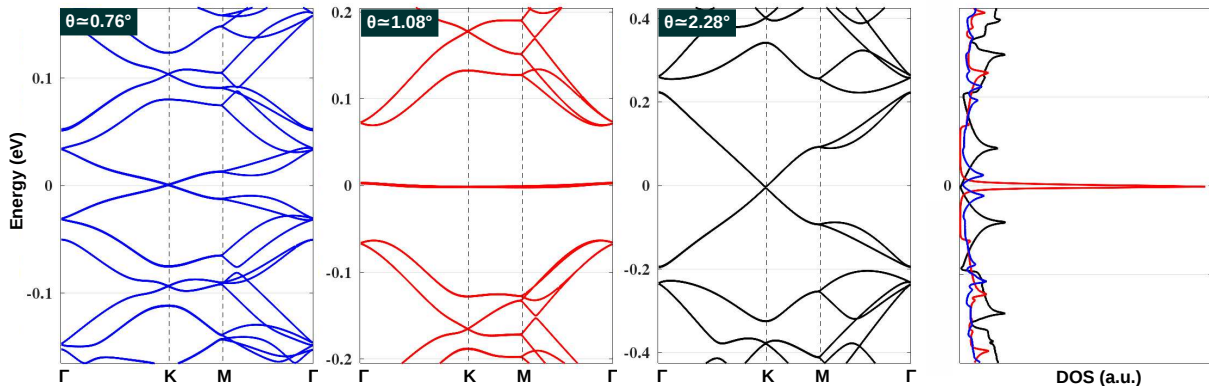


FIG. 3: Electronic bandstructure of TBLG for the twist angle  $\theta < 1.1^\circ$  (left in blue),  $\theta \simeq 1.1^\circ$  (center in red) and  $\theta > 1.1^\circ$  (right in black). The corresponding density of states (DOS) are presented on the extreme right with the same color scale for the three moiré structures.

The structural properties discussed above crucially govern the electronic features of TBLG, as illustrated by the typical electronic structures in Fig.3 as well as the local densities

of states (LDOS) images in Fig.4. In large-angle TBLG, Dirac fermions are still preserved at low energies but a remarkable renormalization of their Fermi velocity is obtained [72], as seen in Fig.3 for  $\theta \simeq 2.28^\circ$ . In addition, saddle points emerge at the crossing of Dirac cones (i.e., at the M-point in the superlattice Brillouin region), yielding van Hove singularities in the density of states (DOS) at energies that are lowered down when decreasing  $\theta$ . When  $\theta$  approaches  $1.1^\circ$ , two (electron and hole) van Hove singularities merge at zero energy and accordingly the low energy bands are flattened, resulting in the observation of an extremely high DOS peak at that energy (see Fig.3 for  $\theta \simeq 1.08^\circ$ ). The angle  $1.1^\circ$  has been thus called the “magic angle” [15]. When further decreasing  $\theta$ , the electronic bands become more dispersive again (see Fig.3 for  $\theta \simeq 0.76^\circ$ ). Remarkably, it has been shown that fully taking the structure relaxation into account, the electronic flat band (accordingly, the localized DOS peak at zero energy) as at  $1.1^\circ$  is no longer observed for small angles  $< 1.1^\circ$  as discussed in details in Ref. [61]. Moreover, even though it is not present in the global electronic quantities, the strong electronic localization is still observed locally in AA stacking regions, which has been experimentally confirmed in Ref. [20].

These distinct electronic properties of TBLG at large and small angles are visually illustrated by the LDOS pictures in Fig.4 as well as their correlation with the structural properties discussed in Fig.2. Actually, the LDOS in Fig.4 are represented in each case at the strongest localization point. First, the strong electronic localization is observed in the AA stacking region for all twist angles. Remarkably, the real-space electronic localization exhibits the similar  $\theta$ -dependence, compared to that of stacking structure presented in Fig.2. Indeed, while it is continuously enlarged when reducing  $\theta$  above  $1.1^\circ$ , the real-space LDOS peak obtained in AA stacking regions is maximum at  $\theta \simeq 1.1^\circ$  and saturates in the regime  $< 1.1^\circ$ . These results demonstrate clearly a strong correlation between the structural properties and the electronic localization features in TBLG.

More remarkably, the observation of electronic flat bands is found to be essentially related to the maximum electronic localization in AA stacking regions and their maximum contribution to the global electronic properties of the system (see also discussions in section V). These features are concurrently obtained at  $\theta \simeq 1.1^\circ$ . To clarify such observation, we notice additionally here that the strongest electronic localization in energy is favorable (unfavorable) in AA stacking regions (other stacking regions) [61]. At large angles  $> 1.1^\circ$ , the electronic localization in AA stacking regions (see Fig.4 for  $\theta \simeq 4.41^\circ$ ) and consequently

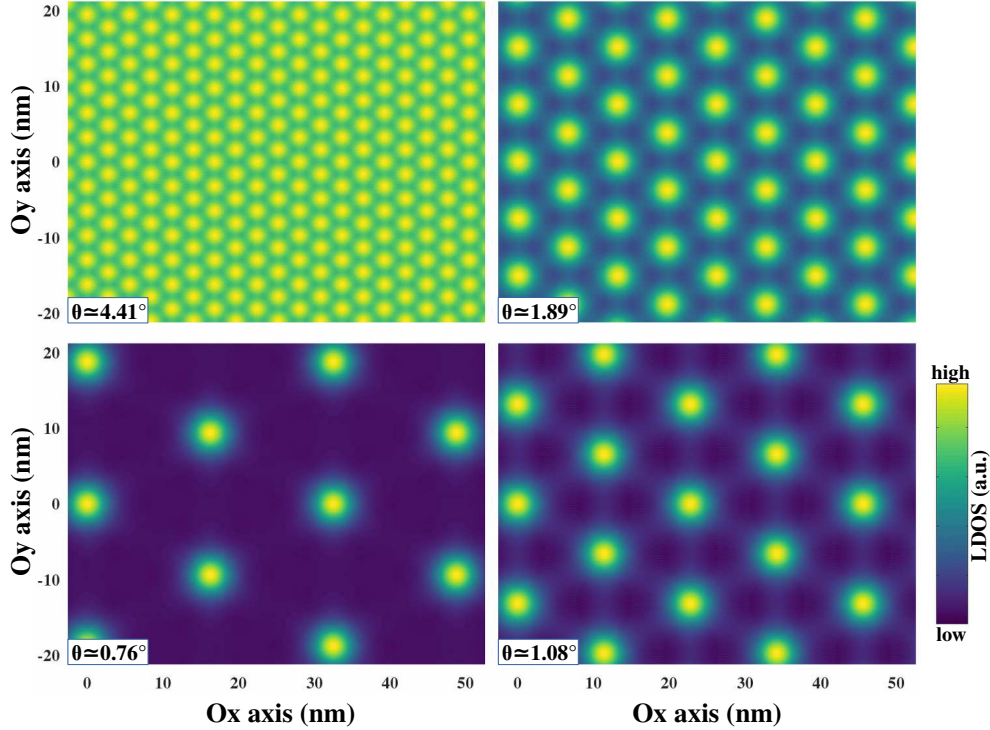


FIG. 4: Real-space LDOS images in TBLG at different twist angles. Energy is fixed where the strongest electronic localization is obtained, i.e., at the van Hove singularity point in DOS (see Fig.3) for  $\theta > 1.1^\circ$  and at zero energy for  $\theta \lesssim 1.1^\circ$ .

the global localization in energy (see the extreme right panel of Fig.3) are relatively weak. When decreasing  $\theta$  in this regime, the electronic localization in AA stacking regions and their contribution are continuously enhanced. Accordingly, global localization (i.e., DOS) peaks increase and their positions concurrently move towards zero energy. At  $\theta \simeq 1.1^\circ$ , all these effects are maximized and consequently the electronic flat bands are obtained. When further decreasing  $\theta$  in the regime below  $1.1^\circ$ , even though a strong electronic localization is still locally observed in the saturated AA stacking region, the increasing contribution of AB/BA stacking ones gradually diminishes the global electronic localization and hence flat bands can not be observed again [61], thus precluding the emergence of other (i.e., small) magic angles predicted by other theoretical calculations [15].

Finally, it is worth noting that even though they could be quantitatively affected by the presence of a larger number of layers and/or by a more complicatedly stacked configuration, the structural and electronic features similar to those presented above are still observed in other TMGs, simply because all these features are essentially governed by twisting effects.

#### IV. TWISTED MULTILAYER GRAPHENE

In this section, the electronic properties of TMGs schematized in Fig.1 are investigated. The creation of these systems could be simply considered as adding one or a few graphene layers to a TBLG one. Since these TMG share a similar  $\theta$ -dependence (e.g., see Refs. [52, 61]) with TBLG, the present study is mainly focused on the magic-angle cases where low-energy bands are most flat and thus strongly correlated electronic phenomena can be observed.

We first consider TMG obtained when one rotated graphene monolayer is placed on top of a graphene multilayer, which is either in an AB-stacked form or an ABC-stacked one (i.e., SM-systems in Fig.1). Fig.5 presents the electronic bandstructures of different SM-systems in both two cases. First of all, the SM-(AB)<sub>2</sub> (i.e., twisted monolayer-bilayer) system at its magic angle exhibits a bandstructure (see on top of Fig.5) with isolated flat bands, similar to that obtained in the magic-angle TBLG. The main difference between two cases is that these bands (accordingly, zero-energy DOS peak) are observed to be less flat (lower) than those of TBLG. Note that continuum Hamiltonian calculations [53] have shown that the bandwidth of flat bands in SM-(AB)<sub>2</sub> system is generally narrower than that obtained in magic-angle TBLG. This is indeed also confirmed by our calculations for systems at the same twist angle in the regime  $\theta \gg 1.1^\circ$ . The results in the magic angle case however exhibit an opposite behavior, i.e., the bandwidth of the magic-angle SM-(AB)<sub>2</sub> system is larger than that obtained in magic-angle TBLG. This is actually consistent with the results presented in Refs. [19, 54] for atomic reconstructed superlattices. These results could be understood as a consequence of the fact, as discussed in the previous section, that the band flatness has a strong correlation with the real-space electronic localization that is basically stronger in AA-stacking regions [61]. In SM-(AB)<sub>2</sub> systems, the corresponding regions are obtained in an AAB-stacked form, i.e., a mixture of AA- and AB-stacking configurations while the latter is unfavorable for the electronic localization. Such mixture diminishes the electronic localization in the SM-(AB)<sub>2</sub> system. This is visibly illustrated by comparing the total LDOS in Fig.6 with that obtained in magic-angle TBLG (see Fig.4 for  $\theta \simeq 1.08^\circ$ ) and is further demonstrated in Fig.14 in section V, thus explaining essentially the less flat bands obtained in the SM-(AB)<sub>2</sub> case.

In addition, another interesting feature is found in Fig.6 that flat bands in the magic-angle SM-(AB)<sub>2</sub> system exhibit a coexistence of layer-resolved localized-delocalized behaviors, i.e.,

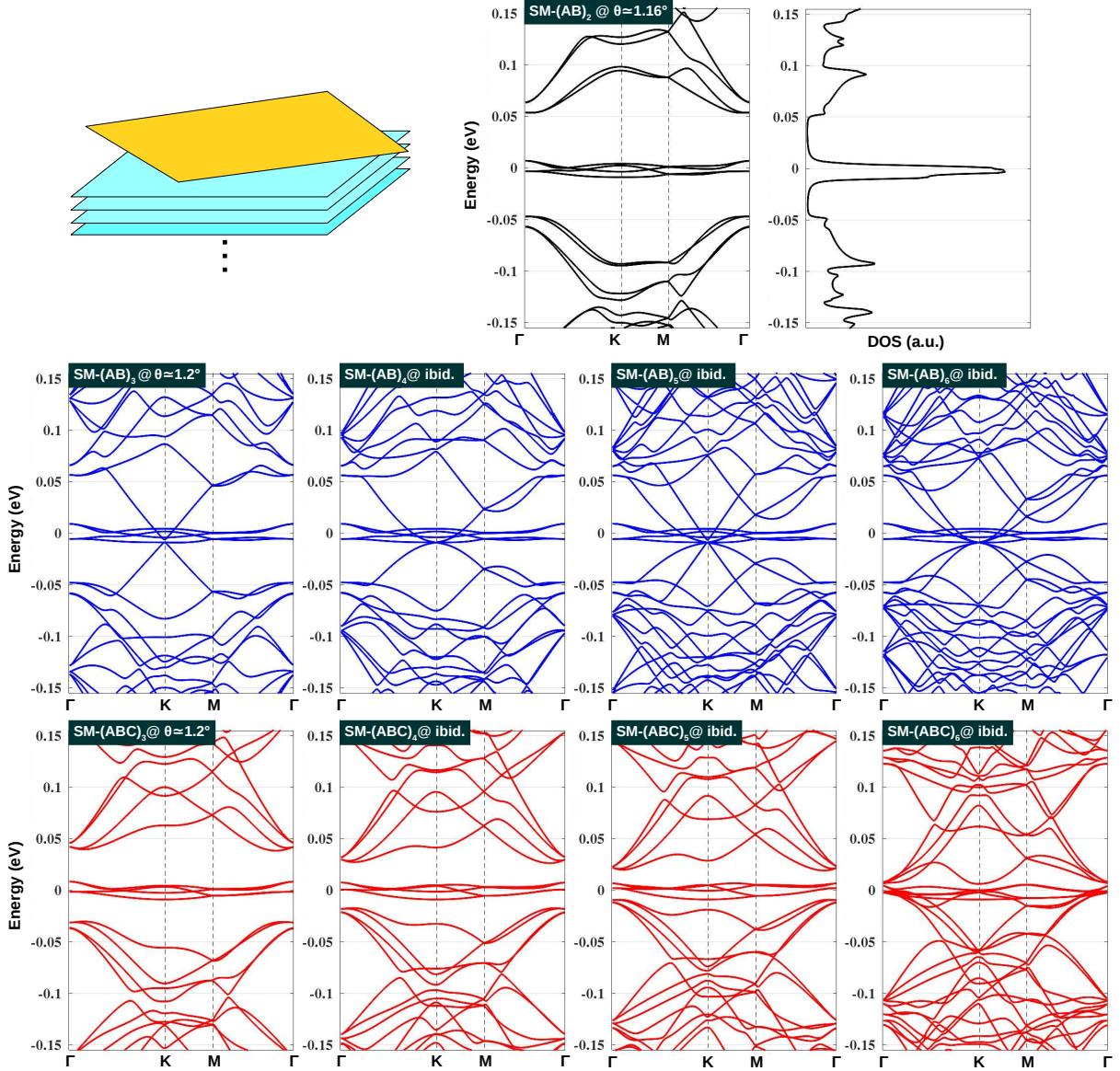


FIG. 5: Electronic bandstructures of different SM-systems at their magic angle. On top, the results in SM-(AB)<sub>2</sub> (i.e., twisted monolayer-bilayer) structure are presented. Other systems including SM-(AB)<sub>n</sub> and SM-(ABC)<sub>n</sub> (see the definition in Fig.1) at their magic angle  $\sim 1.2^\circ$  are computed and presented in the second and third rows, respectively, with  $n = 3, 4, 5, 6$  (from left to right). On top-right, DOS versus energy in SM-(AB)<sub>2</sub> structure is also superimposed.

they are spatially localized on the twisted side whereas delocalized on the bilayer side. This unique feature has been also experimentally confirmed in a recent work [73] and the delocalized correlated electronic states have been similarly explored in twisted double bilayer graphene [74]. Note that electronic states delocalized either in the graphene plane or in

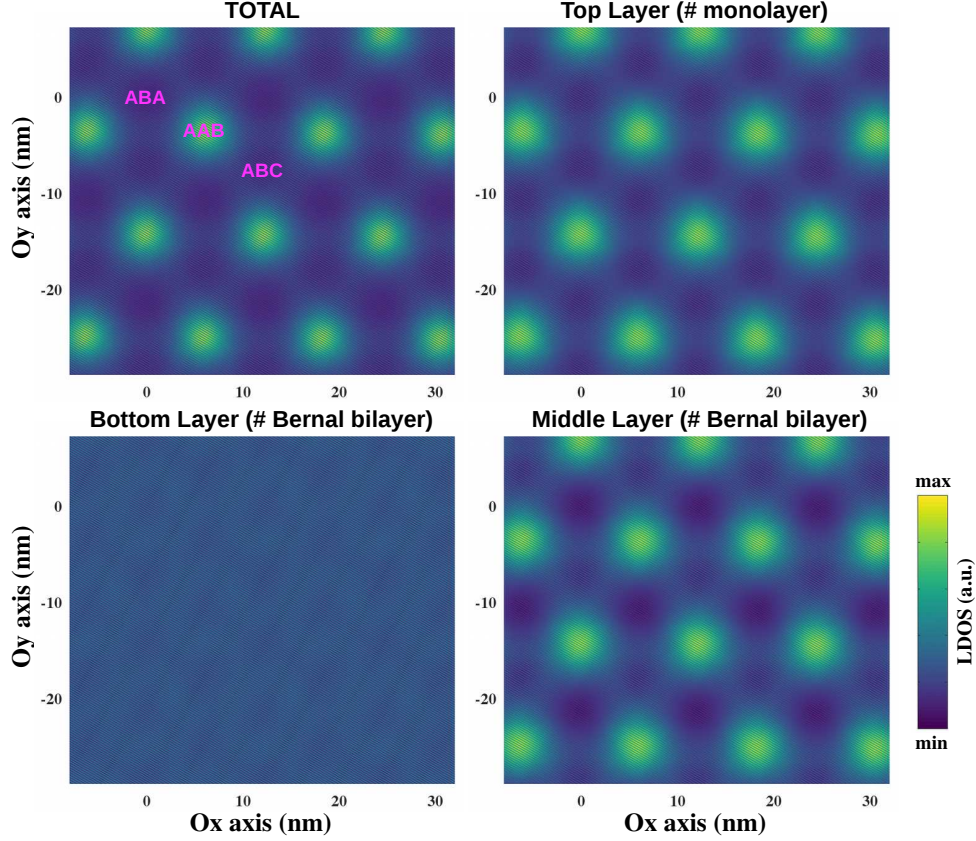


FIG. 6: Total LDOS and layer decomposed LDOS in SM-(AB)<sub>2</sub> system in Fig.5 at zero energy.

different layers are generally obtained in twisted systems consisting of more than 2 layers as the SM-(AB)<sub>2</sub> system here and others considered below, where certain layers are strongly influenced by the moiré superlattice interactions whereas the weak effects take place in other layers. Moreover, the observed coexistence of localized-delocalized electronic states essentially has a tight relationship with the weak real-space localization in the SM-(AB)<sub>2</sub> system discussed above.

When the number of graphene layers of the multilayer counterpart increases, both systems SM-(AB)<sub>n</sub> and SM-(ABC)<sub>n</sub> exhibit clearly distinct electronic properties (see Fig.5). In particular, while the electronic structure of SM-(AB)<sub>n</sub> systems presents both flat bands and dispersive ones at low energies, flat bands in SM-(AB)<sub>n</sub> systems are still clearly isolated from high-energy bands for  $n \leq 5$ . However, the energy gaps between the mentioned bands in the latter case is reduced when increasing  $n$  and is closed for  $n > 5$ . Such distinct properties could be explained by the difference in electronic properties of AB- and ABC-stacked graphene multilayer systems, i.e., while ABC-stacked systems host a single band

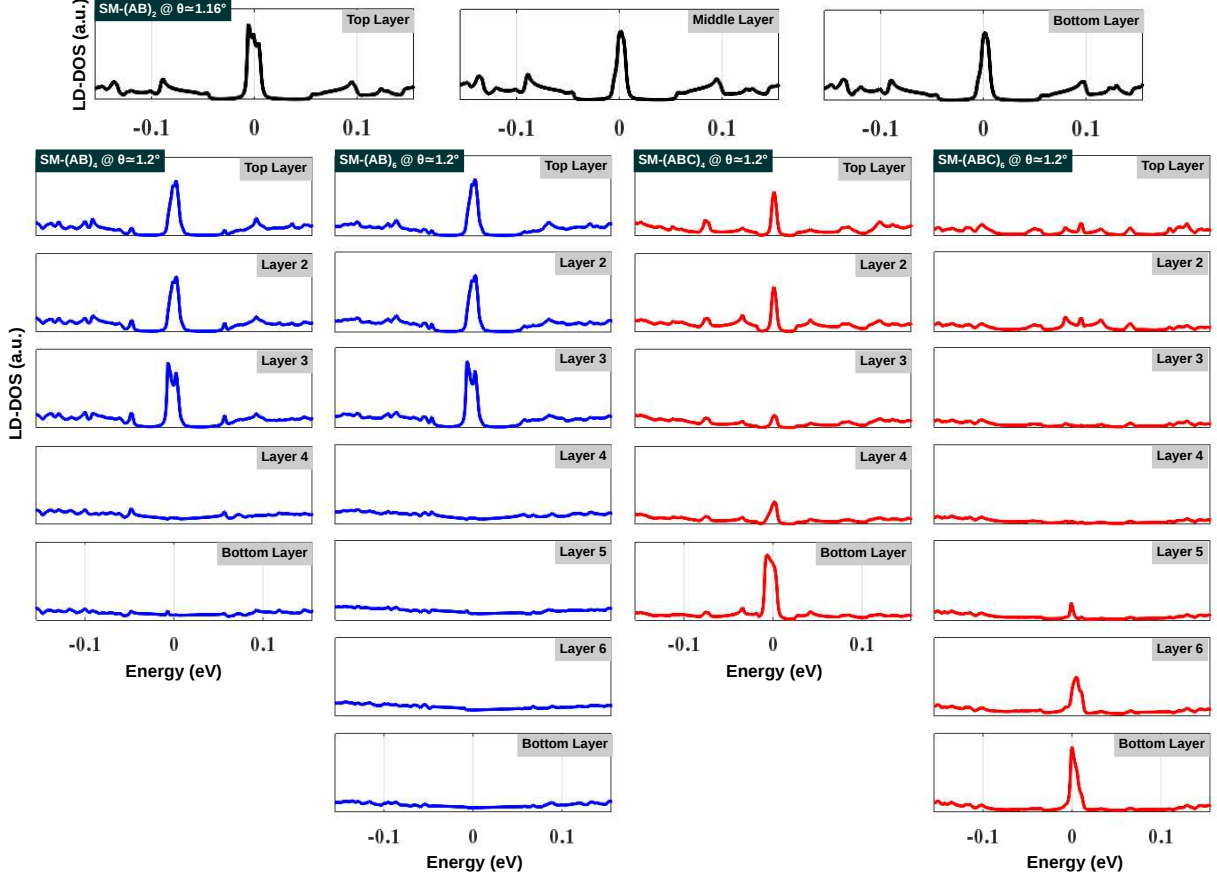


FIG. 7: Layer decomposed DOS (LD-DOS) in some SM-systems considered in Fig.5.

that is partially flat around zero energy, there is a mixture of several (increasing with  $n$ ) parabolic and linear bands in the AB-stacked ones [75].

To further clarify the difference between these two systems, we analyze their layer decomposed DOS (LD-DOS) in function of energy in Fig.7. For the SM-(AB)<sub>2</sub> system, besides the coexistence of layer-resolved localized-delocalized states presented in Fig.6, LD-DOS still exhibits the usual behaviours similar to that observed in magic-angle TBLG. However, other distinct features are found for SM-systems with a larger number of graphene layers. In particular, the electron localization is mostly observed in three top layers of SM-(AB) <sub>$n$</sub>  structures where the moiré superlattice interactions take place. However, the localization is obtained in both top and bottom outermost layers of SM-(ABC)<sub>3</sub> and SM-(ABC)<sub>4</sub> systems (see illustration in Fig.7 for SM-(ABC)<sub>4</sub> one). Moreover, when the number of layers  $n$  further increases, such electron localization in SM-(ABC) <sub>$n$</sub>  surprisingly changes, i.e., the effect in the top outermost layers is diminished while it is enhanced in the bottom ones. When  $n$

is large enough, the electron localization is mostly observed in the bottom outermost layers as illustrated in Fig.7 for the SM-(ABC)<sub>6</sub> system.

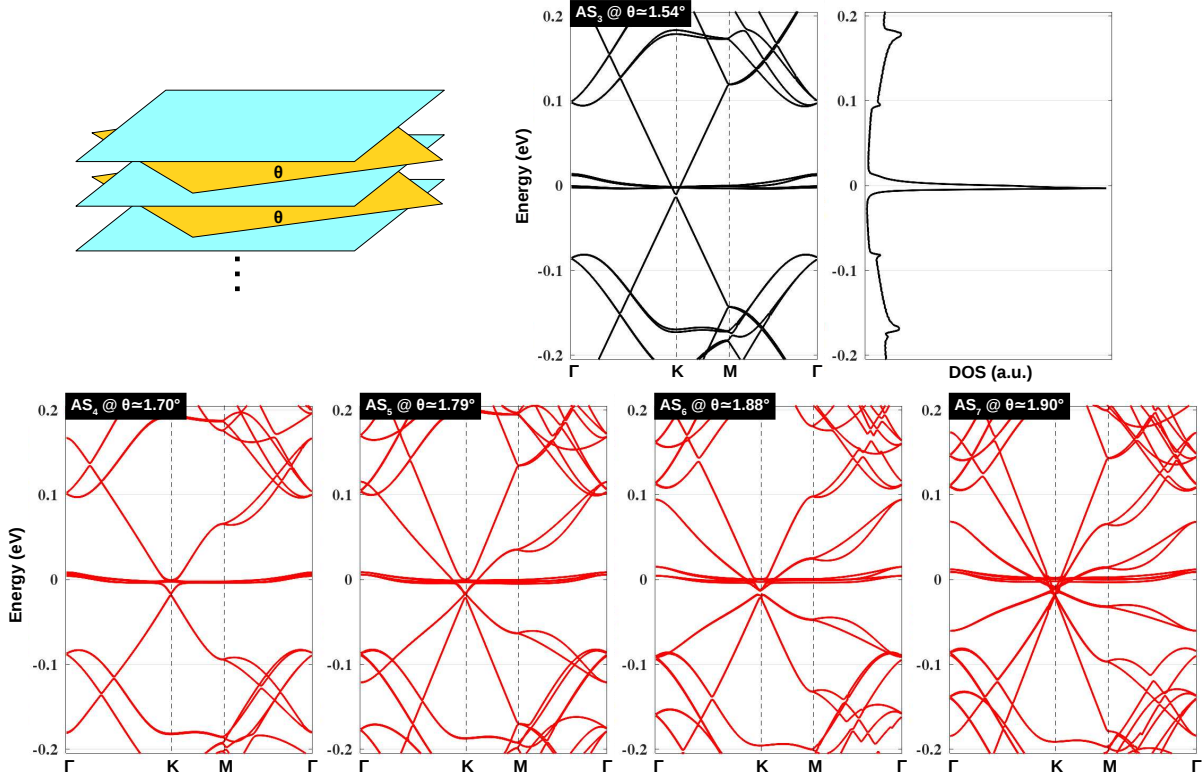


FIG. 8: Electronic bandstructures of alternatively twisted systems of graphene monolayers schematized on top-left (i.e., the  $AS_n$  systems specified in Fig.1) with  $\theta$  near their magic angle  $\theta_n^{MA}$  (see text). On top-right, DOS versus energy in  $AS_2$ -structure is also superimposed.

Next, TMGs created by alternatively rotating  $(0, \theta, 0, \theta, \dots)$  graphene monolayers (i.e.,  $AS_n$  structures in Fig.1) are considered in Fig.8. The magic angle of these  $AS_n$  structures can be estimated by the simple expression  $\theta_n^{MA} = 2\theta_2^{MA} \cos(\pi/(n+1))$  with  $\theta_2^{MA} \simeq 1.1^\circ$  as proposed in Refs. [11, 51]. This is indeed demonstrated in Fig.8 where (almost) flat bands are obtained in  $AS_n$  structures near  $\theta_n^{MA}$ . Different from the results suggested by the effective continuum models [6, 9, 11, 51], the TB bandstructure here presents four degenerate flat bands (more visibly seen in section V when a vertical electric field is applied) and  $n-2$  additional linear bands at low energies. Moreover, saddle points (accordingly, van Hove singularities in DOS) occur in dispersive bands for  $n \geq 4$ . The low-energy bands in these  $AS_n$  systems are also shown to be generally flatter than those obtained for the SM-structures presented in Fig.5, thus confirming again our discussion above about the property of electron

localization in the presence of Bernal stacking bilayer graphene. Note that another difference between systems without and with Bernal stacking bilayer graphene has been also discussed in Ref. [19]. Indeed, in this study, significant sublattice polarization has been observed in the latter case, leading to weaker electron-phonon couplings than those obtained in twisted systems of graphene monolayers only.

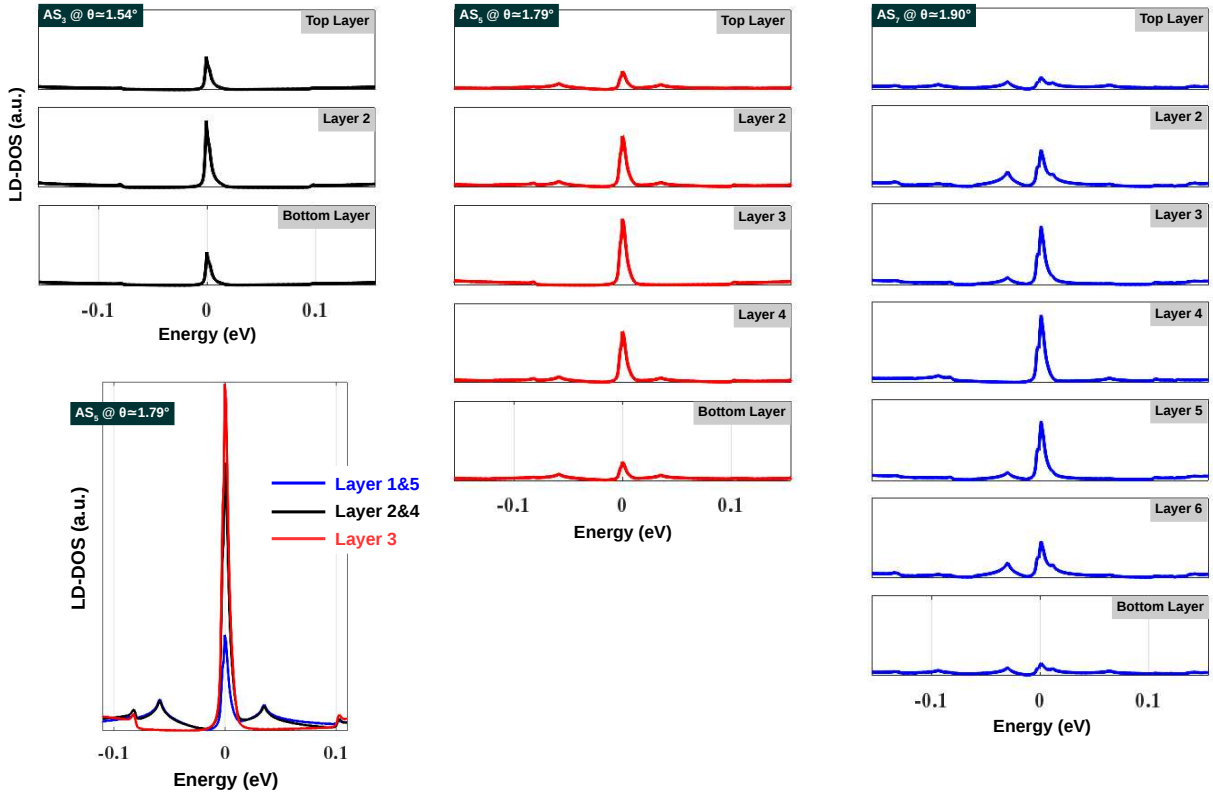


FIG. 9: Layer decomposed DOS (LD-DOS) in some AS-systems considered in Fig.8. On bottom-left, a zoom-combined picture of the results in AS<sub>5</sub> structure is presented.

To understand more deeply their electronic properties, the layer decomposed DOS obtained in these AS<sub>*n*</sub> structures is presented in Fig.9. Remarkably, the strong electronic localization takes place in their centered layers, in contrast to those observed in SM-ones presented in Fig.7. Moreover, LD-DOS in the centered layers presents behaviors that are very similar to those obtained in magic-angle TBLG. In particular, the strongly localized DOS peak is likely isolated from high-energy electronic states by finite energy gaps. Contrastingly, LD-DOS in other layers (especially, the outermost ones) exhibit some signatures of dispersive bands, i.e., the characteristics of linear bands and van Hove singularities induced by the twist as visibly shown in the zoom-image on the bottom of Fig.9. Thus, the

flat bands and dispersive ones of  $AS_n$  structures exhibit oppositely spatial properties, i.e., whereas the former is localized in the system center, the latter is observed in outer layers. This implies that there is also a coexistence of localized-delocalized electronic states in the  $AS_n$  systems of large  $n$ .

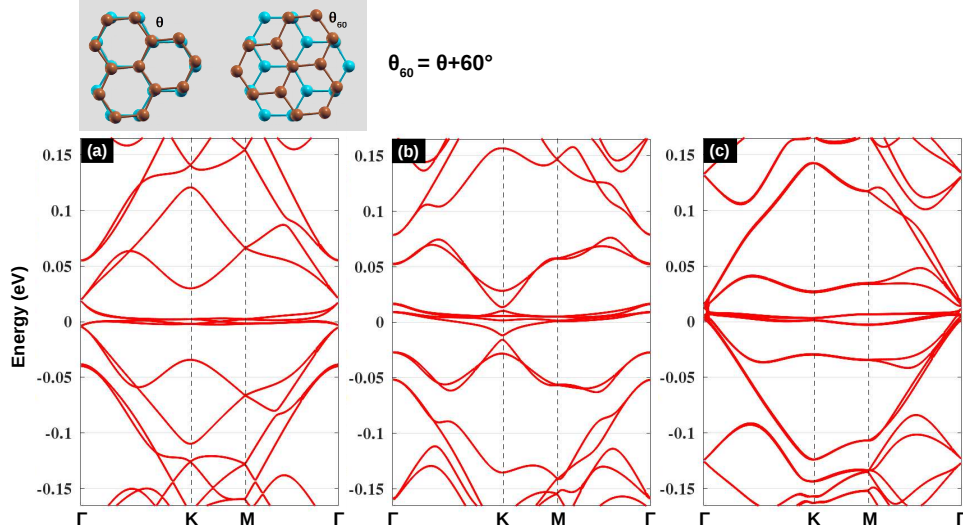


FIG. 10: Electronic bandstructures of  $AS_n$  systems when one or a few layers are additionally rotated by  $60^\circ$  (see the illustration on top). In (a,b), the top layer of  $AS_3$  at  $\theta \simeq 1.30^\circ$  and  $AS_4$  at  $\theta \simeq 1.54^\circ$ , respectively, is additionally rotated by  $60^\circ$ . In (c), such additional  $60^\circ$ -rotation is applied to two top layers of  $AS_4$  at  $\theta \simeq 1.35^\circ$ .

When  $AS_n$  systems are created, another remarkable possibility could in principle be obtained, in particular, one or a few graphene layers are rotated by  $\theta_{60} = \theta + 60^\circ$  (instead of  $\theta$ ) as illustrated on top of Fig.10, similar to that reported in Ref. [76] for graphene/hBN structures. Actually, such  $\theta_{60}$ -rotations do not change the lattice orientation of the graphene layer, compared to the simple  $\theta$ -rotated systems considered in Figs.8-9. However, three AAA-, ABA- and BAB-stacking regions obtained in the latter case are changed to AAB-, ABB- and ABC-stacking ones in the  $AS_n$  systems with  $\theta + 60^\circ$  rotations, leading to significant changes in their electronic structure. Indeed, the flat electronic bands are observed at another twist angle as shown in Fig.10, compared to similar structures (i.e., with the same number of layers) presented in Figs.8-9. In addition, dispersive bands at low energies are generally no longer linear ones. These changes can be clarified by analyzing the structural properties of two considered types of  $AS_n$  systems (e.g., see in Fig.11 for the  $AS_3$  cases). In

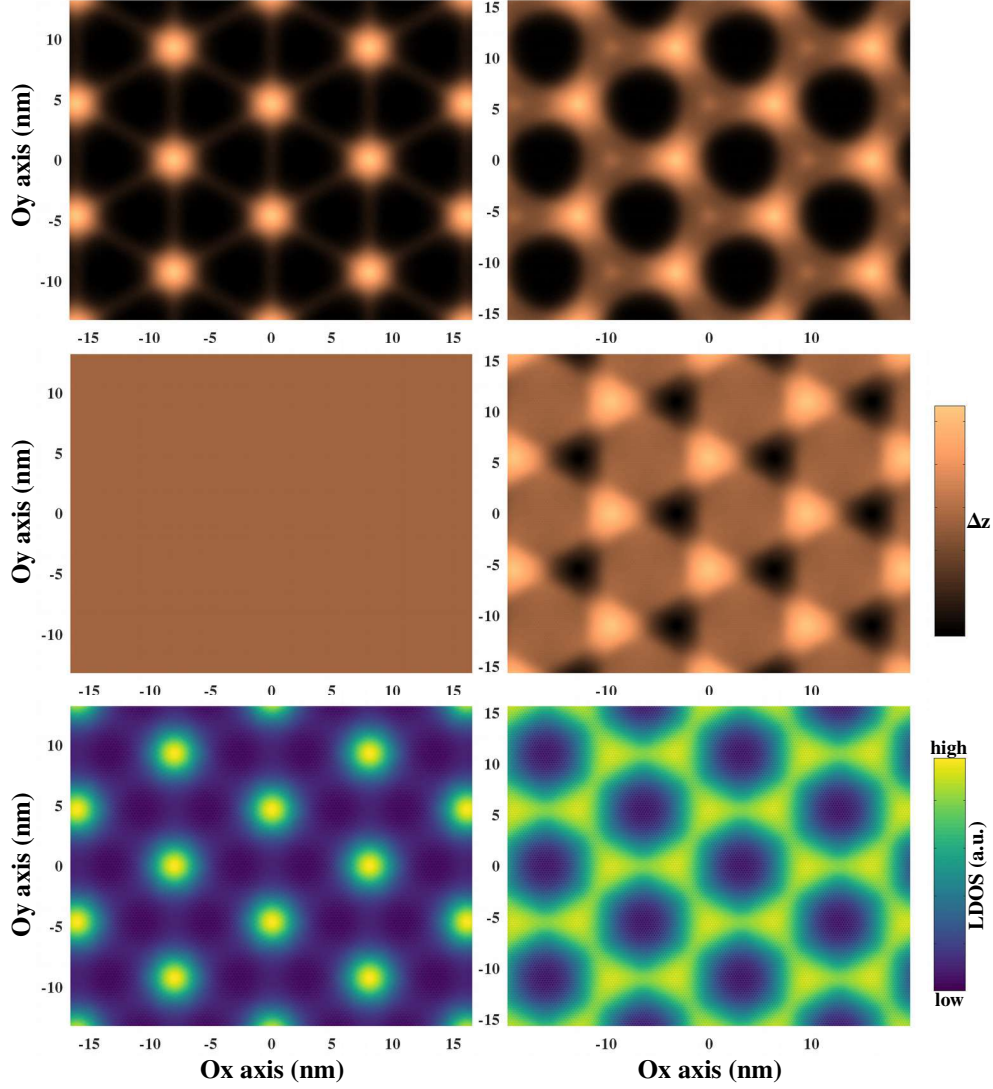


FIG. 11: The structural and electronic properties of two  $\text{AS}_3$  structures:  $\text{AS}_3$  at  $\theta \simeq 1.54^\circ$  in Fig.8 (see in the left) and  $\text{AS}_3$  at  $\theta \simeq 1.30^\circ$  considered in Fig.10a (see in the right). Images in the first and second rows present the spatial variation of out-of-plane displacements in the top and middle layers, respectively. LDOS of two systems at zero energy is presented in the bottom images.

particular, when compared to the first type (i.e., with  $\theta$  rotations only), the top layer of the  $\text{AS}_3$  system in Fig.10a presents a totally different buckling pattern (see the top panels in Fig.11). Similarly, the middle layer of the latter system is no longer flat as that observed in the former one (see the panels in the second row of Fig.11). Accordingly to these different structural properties, these two systems exhibit totally different LDOS images as shown in the bottom of Fig.11. These results thus clarify the difference in their electronic structures

discussed above.

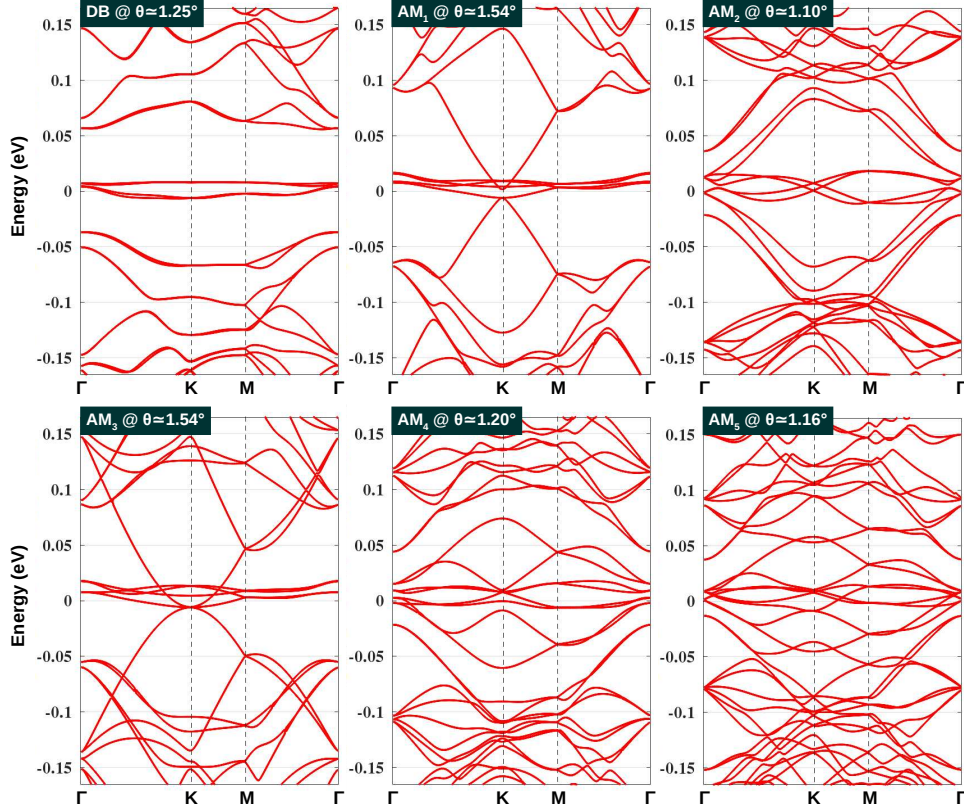


FIG. 12: Electronic bandstructures of TMGs including DB- (i.e., twisted double bilayer graphene) and AM-structures (alternatively twisted structures containing, at least, one Bernal stacking bilayer, as schematized in Fig.1). Calculations were performed at their magic angles where low-energy bands are most flat.

At last, the electronic bandstructures of other TMGs schematized in Fig.1 at their magic angles are presented in Fig.12. First, the isolated flat bands are only obtained in magic-angle DB-structure (i.e., twisted double bilayer graphene) [52], similar to those obtained in TBLG and in SM-(AB)<sub>2</sub> one. AM<sub>n</sub>-systems (n=1,2,3,4,5) are actually alternatively twisted structures but different from the AS ones, containing at least one Bernal stacking bilayer. Most remarkably, the results obtained in those systems show that the flat bands can be easily obtained if the middle layer is a graphene monolayer (i.e., AM<sub>1</sub> and AM<sub>3</sub> structures), whereas the low-energy bands are generally less flat if it is a Bernal stacking bilayer. Moreover, similar to the SM-(AB)<sub>n</sub> and AS<sub>n</sub> structures, dispersive bands are always additionally obtained at low energies, which is likely an inherent property of alternatively twisted systems. Once

more, the low-energy bands of those systems in the presence of Bernal stacking bilayers are shown to be less flat than those presented above for systems of graphene monolayers only.

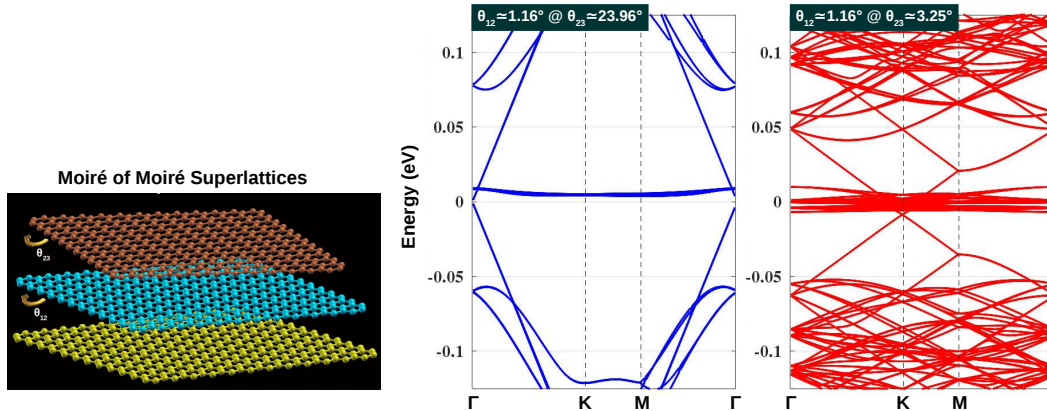


FIG. 13: Electronic bandstructures of moiré of moiré graphene superlattices created by putting one rotated (by  $\theta_{23}$ ) graphene monolayer on top of magic-angle TBLG (i.e.,  $\theta_{12} \simeq 1.08^\circ$ ). Two typical cases, particularly, large angle ( $\theta_{23} \simeq 23.96^\circ$ ) and small angle ( $\theta_{23} \simeq 3.25^\circ$ ), are presented.

For completeness, we finally present in Fig.13 the electronic bandstructures of moiré-of-moiré graphene superlattices, which are here trilayer graphene systems created by vertically stacking magic-angle TBLG (i.e.,  $\theta_{12} \simeq 1.08^\circ$ ) and one rotated (by the angle  $\theta_{23}$ ) graphene monolayer. We particularly consider two cases: a large angle  $\theta_{23} \simeq 23.96^\circ$  and a small one  $\theta_{23} \simeq 3.25^\circ$ . Actually, when  $\theta_{23}$  is large, the interaction between the graphene monolayer and the magic angle TBLG has no significant effect at low energies, i.e., the obtained low-energy bands are approximately a simple combination of the bands of those two systems. Actually, this feature is very similar to those obtained in TBLGs in the large angle regime when their bands can be considered as a combination of the bands of two graphene monolayers. However, when  $\theta_{23}$  is small (i.e.,  $3.25^\circ$  considered here), the mentioned interaction has significant effects on the electronic structure, in particular, the bandwidth of flat bands is significantly enlarged, compared to that obtained in magic-angle TBLG. These results suggest that besides twisted graphene systems investigated above, other more complicated twisted multilayer ones, forming moiré-of-moiré superlattices, shall generally exhibit more complicated electronic structures with less opportunity for observing the flat bands and accordingly, strong electron localization.

## V. FLATTENING ELECTRONIC BANDS AND TUNABILITY

As emphasized in section III, the electronic flat bands in reconstructed TBLG is essentially obtained in the situation when the real-space localization in AA stacking regions and their contribution to the global electronic properties are concurrently maximized at the magic angle. In fact, as it will be demonstrated below, such feature is commonly observed in TMGs and hence could be considered as the practical origin of their observed flat bands.

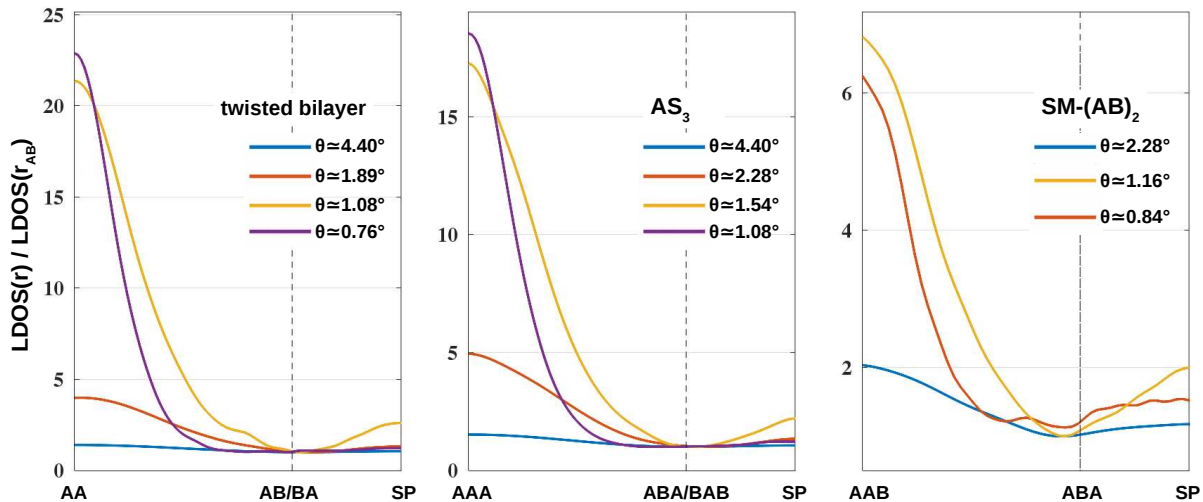


FIG. 14: Spatial variation of LDOS in TBLG,  $AS_3$  and  $SM-(AB)_2$  systems when varying the twist angle around their magic one. The presented LDOS is extracted along the line connecting regions where AA, SP, AB/BA stacking configurations occur. Calculations are performed at energy where the strongest electronic localization is obtained, i.e., at the electron van Hove singularity point for large  $\theta$  and at zero energy for  $\theta$  below the magic angle.

First, it is worth reminding that based on continuum models [15], the first magic angle of TBLG can be estimated using the equation

$$\theta_{MA} \approx 3w/(2\pi t) \quad (2)$$

where  $w$  and  $t$  stand for interlayer and intralayer tunneling strengths, respectively. Indeed,  $\theta_{MA} \approx 1.1^\circ$  is obtained, in very good agreement with experiments [20, 22, 23, 25], with  $w = 0.109$  eV and  $t = 2.7$  eV. Calculations using continuum models [15, 51] have additionally predicted a discrete series of other magic angles  $< 1.1^\circ$ . However, in agreement with the existing experiments (most clearly, see recent articles [20, 22]), atomistic calculations

have demonstrated in Ref. [61] and as discussed in section III that these small magic angles can not be practically obtained in reconstructed TBLGs. This is essentially due to the fact that while it gets maximum at  $\theta \simeq 1.1^\circ$ , the global electronic localization is progressively reduced, according to the increasing contribution of AB/BA stacking regions when reducing  $\theta$  below  $< 1.1^\circ$  as seen in Fig.4 and more visibly in the left-panel of Fig.14. Interestingly, all these features are similarly observed in other TMGs as seen in two examples, i.e.,  $\text{AS}_3$  and  $\text{SM}-(\text{AB})_2$  systems, presented in Fig.14. Indeed, their electronic flat bands (i.e., magic angle) are exactly obtained when the real-space localization in AAA and AAB stacking regions, respectively, and their contribution to the global electronic properties of the system are con-

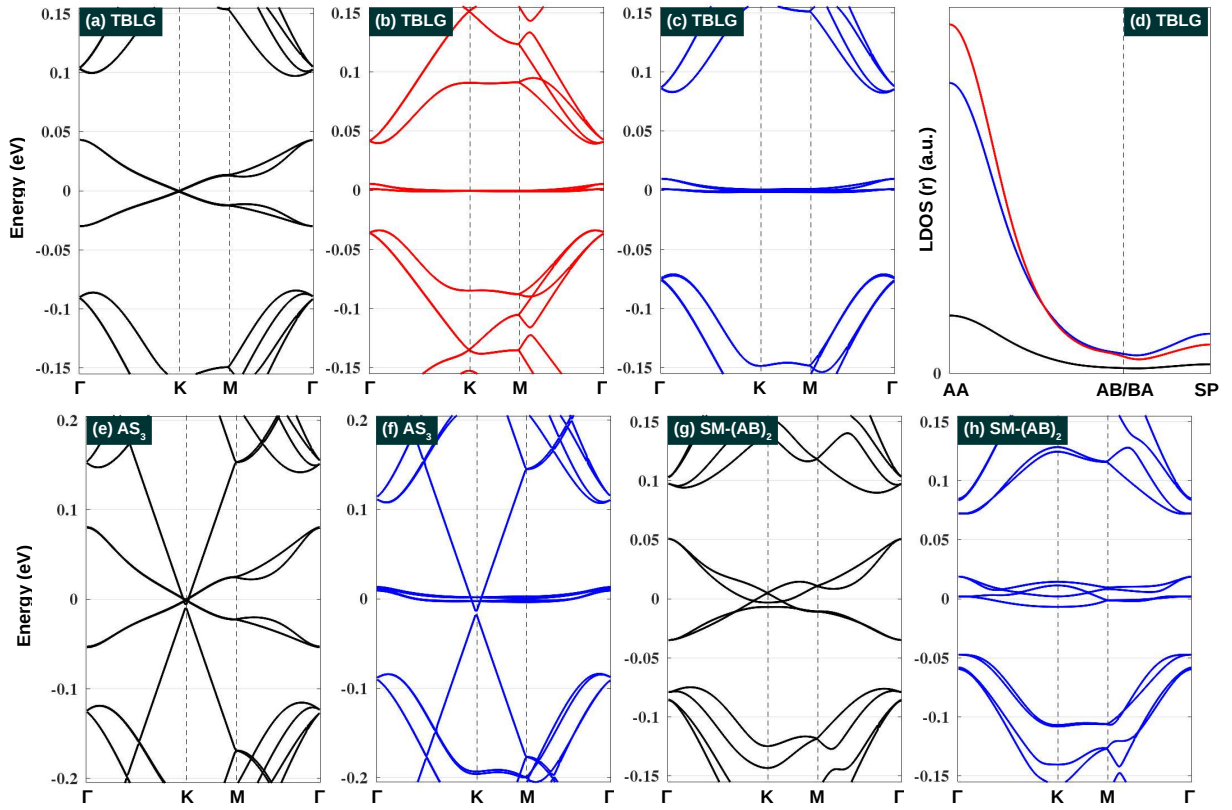


FIG. 15: Electronic structures of TMGs modulated by strain and vertical pressure. TBLG at  $\theta \simeq 1.30^\circ$  is considered in (a) for the pristine case, in (b) with a biaxial strain of 9%, and in (c) with a vertical pressure  $P \simeq 1.45$  GPa. The corresponding LDOS obtained at the strongest electronic localization point is presented in (d). Electronic bandstructures of  $\text{AS}_3$  at  $\theta \simeq 1.89^\circ$  with  $P = 0$  and  $\simeq 2.27$  GPa is displayed in (e) and (f), respectively. The results of  $\text{SM}-(\text{AB})_2$  at  $\theta \simeq 1.47^\circ$  with  $P = 0$  and  $\simeq 2.27$  GPa are in (g) and (h), respectively.

currently maximized. Moreover, the commonness of such observation is further emphasized as it is also valid in TMGs when in-plane strains and/or vertical pressure are applied to tune the magic angle value (see Fig.15 below, especially, the full illustration in Figs.15(a-d)). On the basis of those results, we thus conclude that the maximization of real-space electronic localization in regions where the AA stacking configuration is presented could be considered as the essential origin of the flat electronic bands observed in TMGs.

In addition, the results in Fig.14 are another illustration of feature discussed above that at their magic angles, the real-space electronic localization in the presence of Bernal bilayer graphene (i.e., the SM-(AB)<sub>2</sub> structure here) is significantly weaker than that in the systems of graphene monolayers only. This feature explained why less flat bands (accordingly, smaller localized DOS peak in energy) are obtained in magic-angle systems containing Bernal bilayer graphene, compared to other structures.

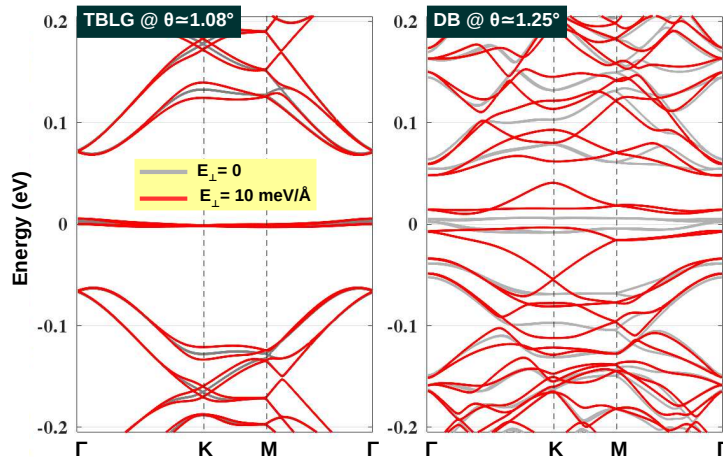


FIG. 16: Effects of vertical electric field  $E_{\perp}$  on the electronic bandstructure of TBLG at  $\theta \simeq 1.08^{\circ}$  and DM-structure at  $\theta \simeq 1.25^{\circ}$ .

As mentioned, the dependence of magic-angle  $\theta_{MA}$  on interlayer and intralayer tunneling strengths described in Eq.(2) suggests that  $\theta_{MA}$  can be tuned by modifying  $w$  and  $t$ , for instance, by applying in-plane strains and vertical pressure [25, 77–82] as illustrated in Fig.15. In particular, the intralayer hopping energies are reduced by a tensile in-plane strain while the interlayer tunneling strength increases when a vertical pressure is applied [83], thus increasing  $\theta_{MA}$  as shown. Even though they could be quantitatively different, these tunable possibilities are commonly obtained in all TMGs as illustrated in Fig.15 for AS<sub>3</sub> and SM-(AB)<sub>2</sub> structures.

Another tunability has been actually explored [4, 5, 8, 54, 55], i.e., by a vertical electric field ( $E$ -field) as illustrated in Figs.16-18. First, Fig.16 presents typical pictures showing the  $E$ -field effects in magic-angle twisted double bilayer graphene (i.e., DB-structure), compared to those in the TBLG structure. It shows that the  $E$ -field generally presents stronger effects in DB-structure than in TBLG one. This could be simply understood as a direct consequence of the fact that  $E$ -field can modulate the bandstructure and open a bandgap in Bernal stacking bilayer graphene, which is not observed for monolayer graphene. These results thus emphasize that vertical  $E$ -field is a good degree of freedom to control the flat band and strongly correlated electronic phenomena in twisted systems containing Bernal stacking bilayer graphene, indeed as reported in Refs. [4, 5, 8, 54, 55].

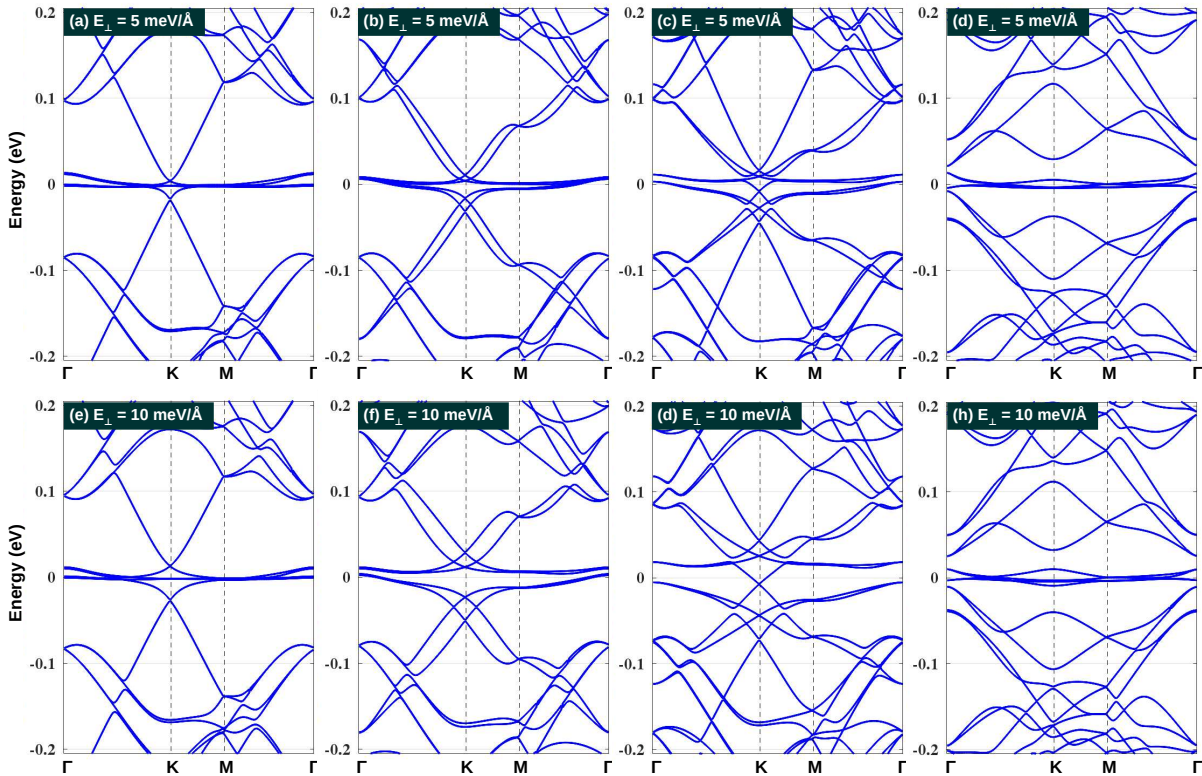


FIG. 17: Electric field ( $E_{\perp}$ ) effects on the electronic bandstructure of  $AS_3$  at  $\theta \simeq 1.54^\circ$  (a,e),  $AS_4$  at  $\theta \simeq 1.70^\circ$  (b,f),  $AS_5$  at  $\theta \simeq 1.79^\circ$  (c,g), and  $AS_3$  considered in Fig.10a at  $\theta \simeq 1.30^\circ$  (d,h).

Alternatively twisted multilayer systems of graphene monolayers (i.e., AS structures) is another example that has shown a good tunability by vertical  $E$ -field [6, 9, 11]. In particular, when an  $E$ -field is applied, a distinct feature observed in AS structures is that the flat bands can strongly hybridize with the Dirac bands, leading to the controllability of the bandwidth

and interaction strength in the flat bands. In Fig.17, the electronic bandstructure of  $AS_n$  ( $n=3,4,5$ ) is presented for two different  $E$ -fields. In addition to the mentioned hybridization, some other interesting effects are found. Indeed, while two flat bands hybridize with two Dirac bands, two other flat bands are still observed in the  $AS_3$  case. For the  $AS_4$  systems, four Dirac bands are observed at low energies (see Fig.8) and hence the hybridization takes place for all four flat bands with these four Dirac bands when a large  $E$ -field is applied. Moreover, the hybridized flat bands can be separated in energy by the  $E$ -field. Similar features occur for  $AS_n$  systems with  $n \geq 5$ , except that besides four Dirac bands hybridizing with flat bands, the remaining Dirac bands are still observed near the Fermi level and a larger separation of hybridized flat bands is obtained.

For the  $AS_n$  structures investigated in Fig.10 when a  $\theta_{60}$  rotation is applied, the  $E$ -field even presents different effects, compared to the conventional cases in Fig.8. In particular, instead of the band hybridization, flat bands in such systems are increasingly isolated from other dispersive bands when an  $E$ -field is applied, as seen in Fig.17(d,h) for the  $AS_3$  system of Fig.10(a). These results could be simply understood by its different structural properties, compared to the conventional  $AS_3$  one of Fig.8 as analyzed in Fig.11.

Finally, to clarify more completely those observed electronic features of  $AS_n$  systems, we

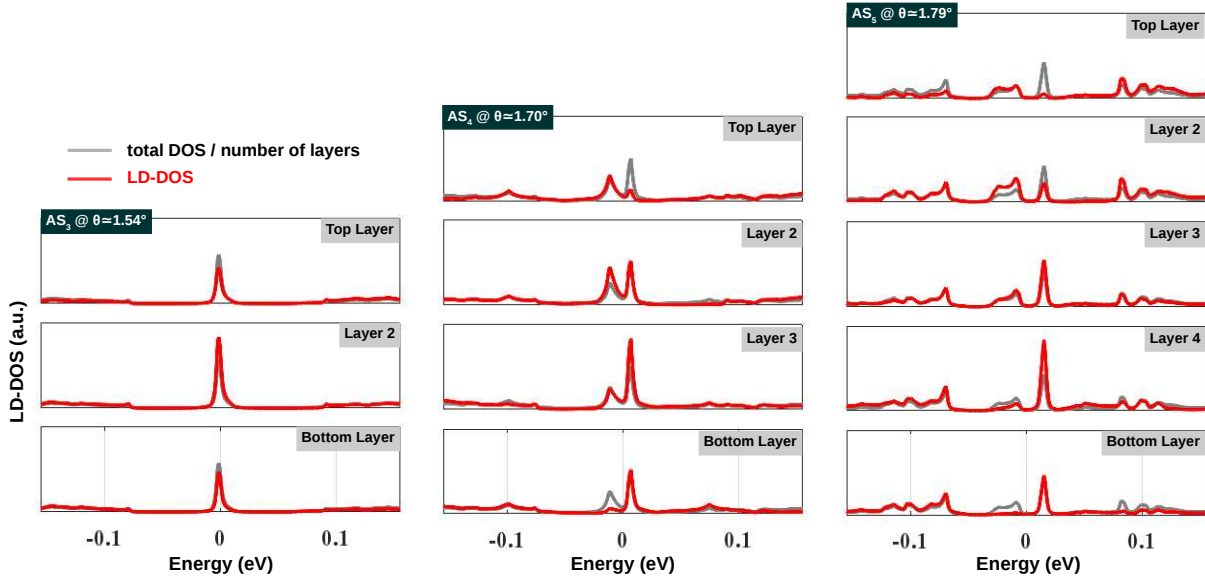


FIG. 18: Layer decomposed DOS (LD-DOS) in systems considered in Figs.17(e-f) when an electric field  $E_{\perp} = 10 \text{ meV}/\text{\AA}$  is applied.

analyze their layer decomposed DOS, when an  $E$ -field is applied, in Fig.18. In the  $AS_3$  case, even though the band hybridization occurs, changes in LD-DOS are relatively weak at the considered  $E$ -fields. This could be because besides two hybridized flat bands, other two flat bands are still preserved near the Fermi level as mentioned above. Stronger  $E$ -field effects on LD-DOS are found in the cases of a larger number of layers. In particular, the single localized DOS peak at zero  $E$ -field is generally separated into two peaks when an  $E$ -field is applied. Interestingly, those two peaks are shown to be likely separated in different layers. Indeed, the electron localized peak is mostly observed in the bottom layers whereas the hole peak in the top ones in the case of  $AS_4$  and  $AS_5$  systems in Fig.18. These results suggest possibilities to control the spatial dependence of electron localization and therefore of strongly correlated electronic phenomena in those twisted systems.

## VI. SUMMARY

Using atomistic calculations, the electronic properties of twisted multilayer graphene systems are systematically studied. First, it is shown that both their structural and electronic properties exhibit a common feature that there is a unique magic angle at which the electronic localization in regions containing AA stacking configuration and its contribution to the global properties of the system are concurrently maximized. Flat electronic bands and strongly correlated electronic phenomena are therefore obtained at this critical case. In addition, the structural and electronic (particularly, electronic localization) properties are shown to exhibit a strong correlation. Consequently, the magic angle separates TMG systems into two classes, i.e., in small and large angle regimes, exhibiting distinct properties as clearly illustrated by the presented results obtained in TBLG [61]. Moreover, the strong correlation between the maximization of electronic localization in AA stacking region and the observation of flat bands presents an unknown physical view about the origin of magic angle. The electronic properties of magic-angle TMGs containing more than 2 graphene layers are shown to exhibit some other distinct properties, due to the presence of a large number of layers as well as various stacking configurations. In particular, the flat bands and dispersive ones at low energies can be concurrently obtained in some structures such as  $SM-(AB)_n$  and alternatively twisted ones. The coexistence of localized-delocalized electronic states spatially separated are observed. At last, these TMGs present good possibilities for tuning electronic

properties by external fields. Finally, the magic angle is also shown to be nicely tunable by the effects of strain and/or vertical pressure. Our study thereby provides a comprehensive overview as well as highlights the essential and outstanding electronic properties of twisted graphene systems that could be helpful for further developments in *twistronics* research.

### Acknowledgments

V.-H.N. and J.-C.C. acknowledge financial support from the Fédération Wallonie-Bruxelles through the ARC Grants (N° 16/21-077 and N° 21/26-116), from the European Union’s Horizon 2020 Research Project and Innovation Program — Graphene Flagship Core3 (N° 881603), from the Flag-Era JTC project “TATTOOS” (N° R.8010.19), from the EOS project “CONNECT” (N° 40007563) and from the Belgium F.R.S.-FNRS through the research projects (N° T.0051.18 and N° T.029.22F). Computational resources have been provided by the CISM supercomputing facilities of UCLouvain and the CÉCI consortium funded by F.R.S.-FNRS of Belgium (N° 2.5020.11). T.X.H. acknowledges support from International Centre of Physics at the Institute of Physics, VAST, under grant number ICP.2022.05.

- 
- [1] Jiang-Bin Wu, Xin Zhang, Mari Ijäs, Wen-Peng Han, Xiao-Fen Qiao, Xiao-Li Li, De-Sheng Jiang, Andrea C. Ferrari, and Ping-Heng Tan. Resonant raman spectroscopy of twisted multilayer graphene. *Nat. Commun.*, 5:5309, 2014.
  - [2] Xu-Dong Chen, Wei Xin, Wen-Shuai Jiang, Zhi-Bo Liu, Yongsheng Chen, and Jian-Guo Tian. High-precision twist-controlled bilayer and trilayer graphene. *Adv. Mater.*, 28:2563–2570, 2016.
  - [3] Umesha Mogera, Sunil Walia, Bharath Bannur, Murali Gedda, and Giridhar U. Kulkarni. Intrinsic nature of graphene revealed in temperature-dependent transport of twisted multilayer graphene. *J. Phys. Chem. C*, 121:13938–13943, 2017.
  - [4] Cheng Shen, Yanbang Chu, QuanSheng Wu, Na Li, Shuopei Wang, Yanchong Zhao, Jian Tang, Jieying Liu, Jinpeng Tian, Kenji Watanabe, Takashi Taniguchi, Rong Yang, Zi Yang Meng, Dongxia Shi, Oleg V. Yazyev, and Guangyu Zhang. Correlated states in twisted double bilayer graphene. *Nat. Phys.*, 16:520–525, 2020.

- [5] Xiaomeng Liu, Zeyu Hao, Eslam Khalaf, Jong Yeon Lee, Yuval Ronen, Hyobin Yoo, Danial Haei Najafabadi, Kenji Watanabe, Takashi Taniguchi, Ashvin Vishwanath, and Philip Kim. Tunable spin-polarized correlated states in twisted double bilayer graphene. *Nature*, 583:221–225, 2020.
- [6] Jeong Min Park, Yuan Cao, Kenji Watanabe, Takashi Taniguchi, and Pablo Jarillo-Herrero. Tunable strongly coupled superconductivity in magic-angle twisted trilayer graphene. *Nature*, 590:249–255, 2021.
- [7] Xi Zhang, Kan-Ting Tsai, Ziyang Zhu, Wei Ren, Yujie Luo, Stephen Carr, Mitchell Luskin, Efthimios Kaxiras, and Ke Wang. Correlated insulating states and transport signature of superconductivity in twisted trilayer graphene superlattices. *Phys. Rev. Lett.*, 127:166802, 2021.
- [8] Shaowen Chen, Minhao He, Ya-Hui Zhang, Valerie Hsieh, Zaiyao Fei, K. Watanabe, T. Taniguchi, David H. Cobden, Xiaodong Xu, Cory R. Dean, and Matthew Yankowitz. Electrically tunable correlated and topological states in twisted monolayer–bilayer graphene. *Nat. Phys.*, 17:374–380, 2021.
- [9] Zeyu Hao, A. M. Zimmerman, Patrick Ledwith, Eslam Khalaf, Danial Haie Najafabadi, Kenji Watanabe, Takashi Taniguchi, Ashvin Vishwanath, and Philip Kim. Electric field–tunable superconductivity in alternating-twist magic-angle trilayer graphene. *Science*, 371:1133–1138, 2021.
- [10] Maria Brzhezinskaya, Oleg Kononenko, Victor Matveev, Aleksandr Zotov, Igor I. Khodos, Vladimir Levashov, Vladimir Volkov, Sergey I. Bozhko, Sergey V. Chekmazov, and Dmitry Roshchupkin. Engineering of numerous moire superlattices in twisted multilayer graphene for twistrionics and straintronics applications. *ACS Nano*, 15:12358–12366, 2021.
- [11] Jeong Min Park, Yuan Cao, Liqiao Xia, Shuwen Sun, Kenji Watanabe, Takashi Taniguchi, and Pablo Jarillo-Herrero. Magic-angle multilayer graphene: A robust family of moire superconductors. *arXiv:2112.10760*, 2021.
- [12] Eva Y. Andrei and Allan H. MacDonald. Graphene bilayers with a twist. *Nat. Mater.*, 19:1265–1275, 2020.
- [13] J. Wang, X. Mu, L. Wang, and M. Sun. Properties and applications of new superlattice: twisted bilayer graphene. *Mater. Today Phys.*, 9:100099, 2019.
- [14] Stephen Carr, Shiang Fang, and Efthimios Kaxiras. Electronic-structure methods for twisted

- moire layers. *Nat. Rev. Mater.*, 5:748–763, 2020.
- [15] Rafi Bistritzer and Allan H. MacDonald. Moire bands in twisted double-layer graphene. *PNAS*, 108:12233–12237, 2011.
- [16] M. Iqbal Bakti Utama, Roland J. Koch, Kyunghoon Lee, Nicolas Leconte, Hongyuan Li, Sihan Zhao, Lili Jiang, Jiayi Zhu, Kenji Watanabe, Takashi Taniguchi, Paul D. Ashby, Alexander Weber-Bargioni, Alex Zettl, Chris Jozwiak, Jeil Jung, Eli Rotenberg, Aaron Bostwick, and Feng Wang. Visualization of the flat electronic band in twisted bilayer graphene near the magic angle twist. *Nat. Phys.*, 17:184–188, 2021.
- [17] Young Woo Choi and Hyoung Joon Choi. Strong electron-phonon coupling, electron-hole asymmetry, and nonadiabaticity in magic-angle twisted bilayer graphene. *Phys. Rev. B*, 98:241412, 2018.
- [18] Alexander Kerelsky, Leo J. McGilly, Dante M. Kennes, Lede Xian, Matthew Yankowitz, Shaowen Chen, K. Watanabe, T. Taniguchi, James Hone, Cory Dean, Angel Rubio, and Abhay N. Pasupathy. Maximized electron interactions at the magic angle in twisted bilayer graphene. *Nature*, 572:95–100, 2019.
- [19] Young Woo Choi and Hyoung Joon Choi. Dichotomy of electron-phonon coupling in graphene moire flat bands. *Phys. Rev. Lett.*, 127:167001, 2021.
- [20] Andreij C. Gadelha, Douglas A. A. Ohlberg, Cassiano Rabelo, Eliel G. S. Neto, Thiago L. Vasconcelos, João L. Campos, Jessica S. Lemos, Vinícius Ornelas, Daniel Miranda, Rafael Nadas, Fabiano C. Santana, Kenji Watanabe, Takashi Taniguchi, Benoit van Troeye, Michael Lamparski, Vincent Meunier, Viet-Hung Nguyen, Dawid Paszko, Jean-Christophe Charlier, Leonardo C. Campos, Luiz G. Cançado, Gilberto Medeiros-Ribeiro, and Ado Jorio. Localization of lattice dynamics in low-angle twisted bilayer graphene. *Nature*, 590:405–409, 2021.
- [21] Andreij C Gadelha, Viet-Hung Nguyen, Eliel G Neto, Fabiano Santana, Markus B Raschke, Michael Lamparski, Vincent Meunier, Jean-Christophe Charlier, and Ado Jorio. Electron-phonon coupling in a magic-angle twisted-bilayer graphene device. *arXiv:2110.14916*, 2021.
- [22] Tiago C Barbosa, Andreij C Gadelha, Douglas A A Ohlberg, Kenji Watanabe, Takashi Taniguchi, Gilberto Medeiros-Ribeiro, Ado Jorio, and Leonardo C Campos. Raman spectra of twisted bilayer graphene close to the magic angle. *2D Mater.*, 9:025007, 2022.
- [23] Yuan Cao, Valla Fatemi, Shiang Fang, Kenji Watanabe, Takashi Taniguchi, Efthimios Kaxiras, and Pablo Jarillo-Herrero. Unconventional superconductivity in magic-angle graphene

- superlattices. *Nature*, 556:43–50, 2018.
- [24] Yuan Cao, Valla Fatemi, Ahmet Demir, Shiang Fang, Spencer L. Tomarken, Jason Y. Luo, Javier D. Sanchez-Yamagishi, Kenji Watanabe, Takashi Taniguchi, Efthimios Kaxiras, Ray C. Ashoori, and Pablo Jarillo-Herrero. Correlated insulator behaviour at half-filling in magic-angle graphene superlattices. *Nature*, 556:80–84, 2018.
- [25] Matthew Yankowitz, Shaowen Chen, Hryhoriy Polshyn, Yuxuan Zhang, K. Watanabe, T. Taniguchi, David Graf, Andrea F. Young, and Cory R. Dean. Tuning superconductivity in twisted bilayer graphene. *Science*, 363:1059–1064, 2019.
- [26] Yonglong Xie, Biao Lian, Berthold Jäck, Xiaomeng Liu, Cheng-Li Chiu, Kenji Watanabe, Takashi Taniguchi, B. Andrei Bernevig, and Ali Yazdani. Spectroscopic signatures of many-body correlations in magic-angle twisted bilayer graphene. *Nature*, 572:101–105, 2019.
- [27] Xiaobo Lu, Petr Stepanov, Wei Yang, Ming Xie, Mohammed Ali Aamir, Ipsita Das, Carles Urgell, Kenji Watanabe, Takashi Taniguchi, Guangyu Zhang, Adrian Bachtold, Allan H. MacDonald, and Dmitri K. Efetov. Superconductors, orbital magnets and correlated states in magic-angle bilayer graphene. *Nature*, 574:653–657, 2019.
- [28] Youngjoon Choi, Jeannette Kemmer, Yang Peng, Alex Thomson, Harpreet Arora, Robert Polski, Yiran Zhang, Hechen Ren, Jason Alicea, Gil Refael, Felix von Oppen, Kenji Watanabe, Takashi Taniguchi, and Stevan Nadj-Perge. Electronic correlations in twisted bilayer graphene near the magic angle. *Nat. Phys.*, 15:1174–1180, 2019.
- [29] Yuhang Jiang, Xinyuan Lai, Kenji Watanabe, Takashi Taniguchi, Kristjan Haule, Jinhai Mao, and Eva Y. Andrei. Charge order and broken rotational symmetry in magic-angle twisted bilayer graphene. *Nature*, 573:91–95, 2019.
- [30] Aaron L. Sharpe, Eli J. Fox, Arthur W. Barnard, Joe Finney, Kenji Watanabe, Takashi Taniguchi, M. A. Kastner, and David Goldhaber-Gordon. Emergent ferromagnetism near three-quarters filling in twisted bilayer graphene. *Science*, 365:605–608, 2019.
- [31] M. Serlin, C. L. Tschirhart, H. Polshyn, Y. Zhang, J. Zhu, K. Watanabe, T. Taniguchi, L. Balents, and A. F. Young. Intrinsic quantized anomalous hall effect in a moire heterostructure. *Science*, 367:900–903, 2020.
- [32] Leon Balents, Cory R. Dean, Dmitri K. Efetov, and Andrea F. Young. Superconductivity and strong correlations in moiré flat bands. *Nat. Phys.*, 16:725–733, 2020.
- [33] Stephen Carr, Daniel Massatt, Shiang Fang, Paul Cazeaux, Mitchell Luskin, and Efthimios

- Kaxiras. Twistronics: Manipulating the electronic properties of two-dimensional layered structures through their twist angle. *Phys. Rev. B*, 95:075420, 2017.
- [34] Kaihui Liu, Liming Zhang, Ting Cao, Chenhao Jin, Diana Qiu, Qin Zhou, Alex Zettl, Peidong Yang, Steve G. Louie, and Feng Wang. Evolution of interlayer coupling in twisted molybdenum disulfide bilayers. *Nat. Commun.*, 5:4966, 2014.
- [35] Peng Kang, Wan-Ting Zhang, Vincent Michaud-Rioux, Xiang-Hua Kong, Chen Hu, Guang-Hua Yu, and Hong Guo. Moiré impurities in twisted bilayer black phosphorus: Effects on the carrier mobility. *Phys. Rev. B*, 96:195406, 2017.
- [36] Mit H. Naik and Manish Jain. Ultraflatbands and shear solitons in moire patterns of twisted bilayer transition metal dichalcogenides. *Phys. Rev. Lett.*, 121:266401, 2018.
- [37] Lede Xian, Dante M. Kennes, Nicolas Tancogne-Dejean, Massimo Altarelli, and Angel Rubio. Multiflat bands and strong correlations in twisted bilayer boron nitride: Doping-induced correlated insulator and superconductor. *Nano Lett.*, 19:4934–4940, 2019.
- [38] Yaping Yang, Jidong Li, Jun Yin, Shuigang Xu, Ciaran Mullan, Takashi Taniguchi, Kenji Watanabe, Andre K. Geim, Konstantin S. Novoselov, and Artem Mishchenko. In situ manipulation of van der waals heterostructures for twistronics. *Sci. Adv.*, 6:eabd3655, 2020.
- [39] Dante M. Kennes, Martin Claassen, Lede Xian, Antoine Georges, Andrew J. Millis, James Hone, Cory R. Dean, D. N. Basov, Abhay N. Pasupathy, and Angel Rubio. Moire heterostructures as a condensed-matter quantum simulator. *Nat. Phys.*, 17:155–163, 2021.
- [40] Qiaoling Xu, Yuzheng Guo, and Lede Xian. Moiré flat bands in twisted 2d hexagonal vdW materials. *2D Mater.*, 9(1):014005, 2021.
- [41] Shengdan Tao, Xuanlin Zhang, Jiaojiao Zhu, Pimo He, Shengyuan A. Yang, Yunhao Lu, and Su-Huai Wei. Designing ultra-flat bands in twisted bilayer materials at large twist angles: Theory and application to two-dimensional indium selenide. *J. Am. Chem. Soc.*, 144:3949–3956, 2022.
- [42] Mengya Liu, Liping Wang, and Gui Yu. Developing graphene-based moire heterostructures for twistronics. *Adv. Sci.*, 9:2103170, 2022.
- [43] Qingjun Tong, Fei Liu, Jiang Xiao, and Wang Yao. Skyrmions in the moire of van der waals 2d magnets. *Nano Lett.*, 18:7194–7199, 2018.
- [44] Chong Wang, Yuan Gao, Hongyan Lv, Xiaodong Xu, and Di Xiao. Stacking domain wall magnons in twisted van der waals magnets. *Phys. Rev. Lett.*, 125:247201, 2020.

- [45] Tiancheng Song, Qi-Chao Sun, Eric Anderson, Chong Wang, Jimin Qian, Takashi Taniguchi, Kenji Watanabe, Michael A. McGuire, Rainer Stöhr, Di Xiao, Ting Cao, Jörg Wrachtrup, and Xiaodong Xu. Direct visualization of magnetic domains and moire magnetism in twisted 2d magnets. *Science*, 374:1140–1144, 2021.
- [46] Xi-Wang Luo and Chuanwei Zhang. Spin-twisted optical lattices: Tunable flat bands and larkin-ovchinnikov superfluids. *Phys. Rev. Lett.*, 126:103201, 2021.
- [47] Wenhui Wang, Wenlong Gao, Xiaodong Chen, Fulong Shi, Guixin Li, Jianwen Dong, Yuanjiang Xiang, and Shuang Zhang. Moire fringe induced gauge field in photonics. *Phys. Rev. Lett.*, 125:203901, 2020.
- [48] Xin-Rui Mao, Zeng-Kai Shao, Hong-Yi Luan, Shao-Lei Wang, and Ren-Min Ma. Magic-angle lasers in nanostructured moire superlattice. *Nat. Nanotechnol.*, 16:1099–1105, 2021.
- [49] Qing Zhang, Guangwei Hu, Weiliang Ma, Peining Li, Alex Krasnok, Rainer Hillenbrand, Andrea Alu, and Cheng-Wei Qiu. Interface nano-optics with van der waals polaritons. *Nature*, 597:187–195, 2021.
- [50] Jialin Chen, Xiao Lin, Mingyuan Chen, Tony Low, Hongsheng Chen, and Siyuan Dai. A perspective of twisted photonic structures. *Appl. Phys. Lett.*, 119:240501, 2021.
- [51] Eslam Khalaf, Alex J. Kruchkov, Grigory Tarnopolsky, and Ashvin Vishwanath. Magic angle hierarchy in twisted graphene multilayers. *Phys. Rev. B*, 100:085109, 2019.
- [52] Fatemeh Haddadi, QuanSheng Wu, Alex J. Kruchkov, and Oleg V. Yazyev. Moiré flat bands in twisted double bilayer graphene. *Nano Lett.*, 20:2410–2415, 2020.
- [53] Youngju Park, Bheema Lingam Chittari, and Jeil Jung. Gate-tunable topological flat bands in twisted monolayer-bilayer graphene. *Phys. Rev. B*, 102:035411, 2020.
- [54] Young Woo Choi and Hyoung Joon Choi. Intrinsic band gap and electrically tunable flat bands in twisted double bilayer graphene. *Phys. Rev. B*, 100:201402, 2019.
- [55] Peter Rickhaus, Folkert K. de Vries, Jihang Zhu, Elías Portoles, Giulia Zheng, Michele Masseroni, Annika Kurzmam, Takashi Taniguchi, Kenji Watanabe, Allan H. MacDonald, Thomas Ihn, and Klaus Ensslin. Correlated electron-hole state in twisted double-bilayer graphene. *Science*, 373:1257–1260, 2021.
- [56] Georgios A Tritsarlis, Stephen Carr, Ziyang Zhu, Yiqi Xie, Steven B Torrisi, Jing Tang, Marios Mattheakis, Daniel T Larson, and Efthimios Kaxiras. Electronic structure calculations of twisted multi-layer graphene superlattices. *2D Mater.*, 7:035028, 2020.

- [57] Stephen Carr, Shiang Fang, Ziyang Zhu, and Efthimios Kaxiras. Exact continuum model for low-energy electronic states of twisted bilayer graphene. *Phys. Rev. Research*, 1:013001, 2019.
- [58] Georgios A Tritsarolis, Stephen Carr, Ziyang Zhu, Yiqi Xie, Steven B Torrisi, Jing Tang, Marios Mattheakis, Daniel T Larson, and Efthimios Kaxiras. Electronic structure calculations of twisted multi-layer graphene superlattices. *2D Mater.*, 7(3):035028, 2020.
- [59] Jiseon Shin, Bheema Lingam Chittari, and Jeil Jung. Stacking and gate-tunable topological flat bands, gaps, and anisotropic strip patterns in twisted trilayer graphene. *Phys. Rev. B*, 104:045413, 2021.
- [60] Fernando Gargiulo and Oleg V Yazyev. Structural and electronic transformation in low-angle twisted bilayer graphene. *2D Mater.*, 5:015019, 2017.
- [61] V. Hung Nguyen, D. Paszko, M. Lamparski, B. van Troeye, V. Meunier, and J.-C. Charlier. Electronic localization in small-angle twisted bilayer graphene. *2D Mater.*, 8:035046, 2021.
- [62] L. Lindsay and D. A. Broido. Optimized tersoff and brenner empirical potential parameters for lattice dynamics and phonon thermal transport in carbon nanotubes and graphene. *Phys. Rev. B*, 81:205441, 2010.
- [63] Aleksey N. Kolmogorov and Vincent H. Crespi. Registry-dependent interlayer potential for graphitic systems. *Phys. Rev. B*, 71:235415, 2005.
- [64] Itai Leven, Tal Maaravi, Ido Azuri, Leor Kronik, and Oded Hod. Interlayer potential for graphene/h-bn heterostructures. *J. Chem. Theory Comput.*, 12:2896–2905, 2016.
- [65] I. Brihuega, P. Mallet, H. González-Herrero, G. Trambly de Laissardière, M. M. Ugeda, L. Magaud, J. M. Gómez-Rodríguez, F. Ynduráin, and J.-Y. Veillen. Unraveling the intrinsic and robust nature of van hove singularities in twisted bilayer graphene by scanning tunneling microscopy and theoretical analysis. *Phys. Rev. Lett.*, 109:196802, 2012.
- [66] Hyobin Yoo, Rebecca Engelke, Stephen Carr, Shiang Fang, Kuan Zhang, Paul Cazeaux, Suk Hyun Sung, Robert Hovden, Adam W. Tsen, Takashi Taniguchi, Kenji Watanabe, Gyu-Chul Yi, Miyoung Kim, Mitchell Luskin, Ellad B. Tadmor, Efthimios Kaxiras, and Philip Kim. Atomic and electronic reconstruction at the van der waals interface in twisted bilayer graphene. *Nat. Mater.*, 18(5):448–453, 2019.
- [67] Shuai Zhang, Aisheng Song, Lingxiu Chen, Chengxin Jiang, Chen Chen, Lei Gao, Yuan Hou, Luqi Liu, Tianbao Ma, Haomin Wang, Xi-Qiao Feng, and Qunyang Li. Abnormal conductivity in low-angle twisted bilayer graphene. *Sci. Adv.*, 6(47):eabc5555, 2020.

- [68] Kazuyuki Uchida, Shinnosuke Furuya, Jun-Ichi Iwata, and Atsushi Oshiyama. Atomic corrugation and electron localization due to moire patterns in twisted bilayer graphenes. *Phys. Rev. B*, 90:155451, 2014.
- [69] Giovanni Cantele, Dario Alfè, Felice Conte, Vittorio Cataudella, Domenico Ninno, and Procolo Lucignano. Structural relaxation and low-energy properties of twisted bilayer graphene. *Phys. Rev. Research*, 2:043127, 2020.
- [70] Michael Lamparski, Benoit Van Troeye, and Vincent Meunier. Soliton signature in the phonon spectrum of twisted bilayer graphene. *2D Mater.*, 7:025050, 2020.
- [71] G. Trambly de Laissardière, D. Mayou, and L. Magaud. Numerical studies of confined states in rotated bilayers of graphene. *Phys. Rev. B*, 86:125413, 2012.
- [72] Long-Jing Yin, Jia-Bin Qiao, Wen-Xiao Wang, Wei-Jie Zuo, Wei Yan, Rui Xu, Rui-Fen Dou, Jia-Cai Nie, and Lin He. Landau quantization and fermi velocity renormalization in twisted graphene bilayers. *Phys. Rev. B*, 92:201408, 2015.
- [73] Ling-Hui Tong, Qingjun Tong, Li-Zhen Yang, Yue-Ying Zhou, Qilong Wu, Yuan Tian, Li Zhang, Lijie Zhang, and Long-Jing Yin Zhihui Qin. Spectroscopic visualization of flat bands in magic-angle twisted monolayer-bilayer graphene: localization-delocalization coexisting electronic states. *arXiv:2109.13528*, 2021.
- [74] Canxun Zhang, Tiancong Zhu, Salman Kahn, Shaowei Li, Birui Yang, Charlotte Herbig, Xuehao Wu, Hongyuan Li, Kenji Watanabe, Takashi Taniguchi, Stefano Cabrini, Alex Zettl, Michael P. Zaletel, Feng Wang, and Michael F. Crommie. Visualizing delocalized correlated electronic states in twisted double bilayer graphene. *Nat. Commun.*, 12:2516, 2021.
- [75] Mikito Koshino. Interlayer screening effect in graphene multilayers with *aba* and *abc* stacking. *Phys. Rev. B*, 81:125304, 2010.
- [76] Nathan R. Finney, Matthew Yankowitz, Lithurshanaa Muraleetharan, K. Watanabe, T. Taniguchi, Cory R. Dean, and James Hone. Tunable crystal symmetry in graphene–boron nitride heterostructures with coexisting moiré superlattices. *Nat. Nanotechnol.*, 14:1029–1034, 2019.
- [77] V Hung Nguyen and P Dollfus. Strain-induced modulation of dirac cones and van hove singularities in a twisted graphene bilayer. *2D Mater.*, 2:035005, 2015.
- [78] Loïc Huder, Alexandre Artaud, Toai Le Quang, Guy Trambly de Laissardière, Aloysius G. M. Jansen, Gérard Lapertot, Claude Chapelier, and Vincent T. Renard. Electronic spectrum of

- twisted graphene layers under heterostrain. *Phys. Rev. Lett.*, 120:156405, 2018.
- [79] Xianqing Lin, Haotian Zhu, and Jun Ni. Pressure-induced gap modulation and topological transitions in twisted bilayer and twisted double bilayer graphene. *Phys. Rev. B*, 101:155405, 2020.
- [80] Yi-Wen Liu, Ying Su, Xiao-Feng Zhou, Long-Jing Yin, Chao Yan, Si-Yu Li, Wei Yan, Sheng Han, Zhong-Qiu Fu, Yu Zhang, Qian Yang, Ya-Ning Ren, and Lin He. Tunable lattice reconstruction, triangular network of chiral one-dimensional states, and bandwidth of flat bands in magic angle twisted bilayer graphene. *Phys. Rev. Lett.*, 125:236102, 2020.
- [81] Zewen Wu, Xueheng Kuang, Zhen Zhan, and Shengjun Yuan. Magic angle and plasmon mode engineering in twisted trilayer graphene with pressure. *Phys. Rev. B*, 104:205104, 2021.
- [82] Bálint Szentpéteri, Peter Rickhaus, Folkert K. de Vries, Albin Márffy, Bálint Fülöp, Endre Tóvári, Kenji Watanabe, Takashi Taniguchi, Andor Kormányos, Szabolcs Csonka, and Péter Makk. Tailoring the band structure of twisted double bilayer graphene with pressure. *Nano Lett.*, 21:8777–8784, 2021.
- [83] To model the effects of vertical pressure  $P$ , the average interlayer distance  $d$  is fixed and modified (in relaxation simulations) with respect to its equilibrium value  $d_0$ . The same approach is applied to superlattice vectors to model in-plane strains.  $P$  is estimated as in Phys. Rev. B 98, 085144 (2018), i.e.,  $P = A(e^{-B\epsilon} - 1)$  with  $A = 5.73$  GPa,  $B = 9.54$ , and  $\epsilon = 1 - (d/d_0)$ .